Title
Dispatched uses Na+ flux to power release of lipid-modified Hedgehog

Journal
Nature, 599(7884)

ISSN
0028-0836

Authors
Wang, Qianqian
Asarnow, Daniel E
Ding, Ke
et al.

Publication Date
2021-11-11

DOI
10.1038/s41586-021-03996-0

Peer reviewed

Published in final edited form as:

Nature. 2021 November ; 599(7884): 320–324. doi:10.1038/s41586-021-03996-0.

Dispatched uses Na^+ flux to power lipid-modified Hedgehog release

Qianqian Wang[1,†], **Daniel E. Asarnow**[2,†], **Ke Ding**[1], **Randall Mann**[1], **Jason Hatakeyama**[1], **Yunxiao Zhang**[1,‡], **Yong Ma**[3,§], **Yifan Cheng**[2,4,*], **Philip A. Beachy**[1,5,*]

[1]Institute for Stem Cell Biology and Regenerative Medicine, Stanford University School of Medicine, Stanford, California 94305, USA

[2]Department of Biochemistry and Biophysics, University of California, San Francisco, California 94158, USA

[3]Department of Molecular Biology and Genetics, Johns Hopkins University School of Medicine, Baltimore, CA 21205

[4]Howard Hughes Medical Institute, University of California, San Francisco, California 94158, USA

[5]Departments of Urology, and Developmental Biology, Stanford University School of Medicine, Stanford, California 94305, USA

Abstract

The Dispatched protein, which is related to the NPC1 and PTCH1 cholesterol transporters[1,2] and to H^+-driven transporters of the RND family[3,4], enables tissue-patterning activity of the lipid-modified Hedgehog protein by releasing it from tightly -localized sites of embryonic expression[5–10]. Here we determine a cryo-electron microscopy structure of the mouse protein Dispatched homologue 1 (DISP1), revealing three Na^+ ions coordinated within a channel that traverses its transmembrane domain. We find that the rate of Hedgehog export is dependent on the Na^+ gradient across the plasma membrane. The transmembrane channel and Na^+ binding are disrupted in DISP1-NNN, a variant with asparagine substitutions for three intramembrane aspartate residues that each coordinate and neutralize the charge of one of the three Na^+ ions.

Correspondence and requests for materials should be addressed to Yifan Cheng or Philip A. Beachy. *Corresponding author. yifan.cheng@ucsf.edu (Y.C.), pbeachy@stanford.edu (P.A.B.).

§Current address: Suzhou Institute of Biomedical Engineering and Technology, Chinese Academy of Sciences, 88 Keling Road, SND, Suzhou, Jiangsu 215163, China

‡Current address: Howard Hughes Medical Institute, Neuroscience Department, The Scripps Research Institute, La Jolla, CA 92037, USA.

†These authors contributed equally to this work.

Author contributions

Q.W. purified and characterized DISP1-A, DISP1-A-NNN and ShhN-DISP1-A complex and SCUBE2 protein, and developed and performed ShhNp binding and release assays. D.E.A. prepared cryo-EM grids, collected and processed cryo-EM data, and performed the 3DVA. R.M. devised and aided the SCUBE2 purification. J.H. performed ShhNp release assays. K.D., D.E.A., Y.Z., and Q.W. built the models. Y.M. provided mouse genetic epistasis analysis while in the laboratory of P.A.B. at Johns Hopkins University School of Medicine. All authors participated in discussion and analysis of the data. P.A.B., Q.W., D.E.A., K.D., Y.C., and Y.Z. prepared the manuscript.

Competing interests The authors declare no competing interests.

Supplementary Information The online version contains supplementary material available at https://doi.org/10.1038/s41586-021-03996-0.

DISP1-NNN and variants that disrupt single Na^+ sites retain binding to, but are impaired in export of the lipid-modified Hedgehog protein to the SCUBE2 acceptor. Interaction of the amino-terminal signalling domain of the Sonic hedgehog protein (ShhN) with DISP1 occurs via an extensive buried surface area and contacts with an extended furin-cleaved DISP1 arm. Variability analysis reveals that ShhN binding is restricted to one extreme of a continuous series of DISP1 conformations. The bound and unbound DISP1 conformations display distinct Na^+-site occupancies, which suggests a mechanism by which transmembrane Na^+ flux may power extraction of the lipid-linked Hedgehog signal from the membrane. Na^+-coordinating residues in DISP1 are conserved in PTCH1 and other metazoan RND family members, suggesting that Na+ flux powers their conformationally driven activities.

During embryogenesis, the Hedgehog signal projects its tissue-patterning influence many cells beyond its sites of expression in ‘organizers’ such as the vertebrate notochord, the floor plate of the neural tube and the zone of polarizing activity in the developing limb[11–14]. The mature Sonic hedgehog protein signal (ShhNp) is covalently lipid-modified[15] by autoprocessing-mediated cholesterol attachment at its C terminus[16] and acyl transferase-mediated attachment of palmitate at its N terminus[17,18]. The resulting dual-lipid-modified protein is tightly membrane associated and thus requires dedicated machinery for its packaging and release in long-range patterning. This machinery includes the DISP1[5–10], which is required in Hedgehog-producing cells, and SCUBE, a secreted protein that can be supplied by other cells that do not produce or respond to the Hedgehog signal[19–21]. Although DISP1 and the related Hedgehog receptor PTCH1 are similar in sequence and transmembrane topology and both interact with the lipid-modified Hedgehog signal, DISP1-mediated Hedgehog release promotes Hedgehog pathway activity, whereas PTCH1 attenuates this activity by inhibiting the essential response component Smoothened (SMO) (Extended Data Fig. 1a, b, Supplementary Discussion).

DISP1 structure determination

We determined the structure of a stable, functional N-terminal truncation of DISP1 (DISP1-A) (Extended Data Figs. 1c–e, 2). Monomeric DISP1-A purified into a mixture of lauryl maltose neopentyl glycol (LMNG), glyco-diosgenin (GDN) and cholesteryl hemisuccinate (CHS) was efficiently cleaved at an essential furin site22 (Extended Data Fig. 1f), and 3D classification of a single-particle cryo-EM dataset revealed high-resolution structures of two major classes—relaxed (R) (2.5 Å resolution); and tense (T) (2.5 Å resolution)—each comprising at least two subclasses (Extended Data Figs. 3, 4, Extended Data Table 1). We further applied 3D variability analysis23 (3DVA; Methods), to systematically model the conformational landscape within our dataset as a series of orthonormal principal components representing specific modes of motion. We found conformations resembling R and T at opposite ends of the second principal component (PC2) of this dataset (Extended Data Fig. 5, Supplementary Video 1), and we present a model of DISP1-A built from the density of R.

DISP1-A structure resembles that of PTCH1, with twelve transmembrane helices (TM1–TM12) derived from apparent duplication of a six-transmembrane-helix unit (TM1–TM6 and TM7–TM12) arranged in pseudodyad symmetry and preceded by amphipathic

transverse helices at the cytoplasmic membrane surface (pre-TM1 and pre-TM7). Each unit contains a large extracellular loop derived from corresponding positions between TM1 and TM2 and between TM7 and TM8 (Fig. 1a, b).

Unlike the extracellular domains (ECDs) of PTCH1, which are juxtaposed to form a conduit for sterol transport1, the mouse DISP1 ECDs are splayed apart in a Y-shaped manner (Fig. 1a), as also recently reported for Drosophila Disp24 and human DISP125. DISP1 also resembles PTCH1 in the presence of ferredoxin-like α + β open-faced sandwich folds in the membrane-proximal parts of ECD1 and ECD2 (Extended Data Fig. 1g).

Each ECD accepts secondary structure elements from the other loop, enclosing a bowl-shaped space between the two domains. The linker within the TM1–TM2 loop is the site of furin cleavage[22] (Arg276-Glu-Arg-Arg279), opening the bowl at a location we designate as ‘front’. The ECDs contain seven disulfide bonds, five in ECD1 and two in ECD2 (Fig. 1b, Extended Data Figs. 2, 6), and five N-linked glycosylation sites (Fig. 1b, Extended Data Figs. 1g, 2). Except for pre-TM1 and pre-TM7, most intracellular sequence in DISP1-A is not resolved, including four N-terminal residues (1, 2, 172 and 173), 14 residues preceding pre-TM7 (667–680) and 378 residues at the C terminus (1144–1521). In the ECDs, 19 residues including the furin cleavage site (264–282) and residues 399–409 are not resolved.

We modelled 28 lipid or detergent molecules, mostly at annular positions around the transmembrane domain. Twenty-six of these molecules were CHS, 17 corresponding to the inner leaflet and 9 to the outer leaflet of the membrane, presenting the appearance of a sterol bilayer (Fig. 1c, Supplementary Video 2). Two of the nine outer leaflet sterols were raised, and the front-side lifted sterol may correspond to an intermediate state in ShhNp export (see below)—a nearby lipidic group, modelled as LMNG, levers the lifted sterol upward (Fig. 1c, Supplementary Video 2).We also modelled a non-proteogenic density within a hydrophobic cavity at the distal tip of ECD2 as an LMNG molecule (Fig. 1c, Supplementary Video 2).

Na^+ ions in a transmembrane tunnel

The transmembrane domain contained three non-proteogenic densities (sites I, II and III), each associated with one of the three acidic residues in TM4 and TM10 that are conserved in PTCH1 (Fig. 2a, Extended Data Fig. 7a–c). These densities appear to be metal cations, well-coordinated by oxygens from side-chain hydroxyls and main-chain carbonyls, and at least one oxygen from water (site III) (Fig. 2a). Site I and II cations lie on the axis of pseudodyad symmetry between TM1–TM6 and TM7–TM12, each receiving coordination bonds from symmetry-related oxygens in both opposing six-transmembrane helix units. The site III cation is asymmetrically positioned, its ligands deriving entirely from TM4 and TM5.

The coordination number is 5 for sites I and II and 6 for site III, the centre-to-centre distances between ions and their associated oxygens averaging 2.50 Å, 2.51 Å, and 2.47 Å, respectively. Each density in these three sites is associated with a single carboxylate and with oxygens from hydroxyls and main chain carbonyls, ruling out alkaline earth metal ions such as Ca^{2+} or Mg^{2+}, which require additional charge neutralization, display a more rigid geometry and a tighter coordination sphere, and are rarely coordinated by main-chain

carbonyls. The average bond distances match those characteristic[26] of Na^+ (2.4–2.5 Å) rather than K^+ (2.7–3.2 Å). We therefore conclude that the densities at sites I, II and III derive from Na^+, as further validated by the CheckMyMetal web server[26].

To assess the role of Na+ in DISP1 activity, we modified a quantitative assay for release of ShhNp[6] by: (1) replacing luciferase between amino acid residues 131 and 132 of Shh with nanoluciferase (Extended Data Fig. 8a); (2) use of DISP1-A–mEGFP (Extended Data Fig. 1c); and (3) use of purified SCUBE2 protein in defined medium as the acceptor (Extended Data Fig. 8b, c). This assay provides a rapid, quantitative measure of the rate of nanoluciferase (nanoLuc)–ShhNp release into the medium over a period of minutes (Extended Data Fig. 8d). Under reduced Na^+, with the organic cation N-methyl-d-glucamine ($NMDG^+$) used to maintain osmolarity[27], we found that release by DISP1-A activity ranged from near zero at 10 mM extracellular Na^+ to partial and full restoration of release at extracellular Na^+ concentrations of 40 and 155 mM (Fig. 2b, Extended Data Fig. 8d); a similar observation was reported during revision of our manuscript[28].

Mutation of DISP1-A D571, D572 and D1049—the charge-neutralizing residues in TM4 and TM10—to asparagine, resulting in DISP1-A-NNN, caused disruption of ShhNp release (Fig. 2c) in vitro, as previously established in vivo[6]. Disruption of sites I, II and III individually also disrupted release of ShhNp (Fig. 2c, Extended Data Fig. 8e). Given that all of these variant proteins are stable and retain the ability to bind ShhNp (Extended Data Fig. 8f), the results indicate that Na^+ coordination is critical for ShhNp release.

Utilization of a Na^+ gradient to power DISP1 activity implies Na^+ flux across the membrane. We found a path extending from the extracellular surface of the DISP1 transmembrane domain to the intracellular surfaces[29]; most water molecules within the transmembrane domain were clustered near this channel (Fig. 3a, Supplementary Video 3). We determined the structure of DISP1-A-NNN at 3.2 Å resolution (Extended Data Fig. 3, Extended Data Table 1), revealing that the Na^+ ion densities at sites I, II and III are indeed absent (Fig. 3b), and the side chains of the asparagine residues substituted for aspartates and some of the remaining liganding side chains are rearranged (Fig. 3b) compared with the wild-type protein. We compared water-excluded internal cavities within the transmembrane domains of these proteins (Extended Data Fig. 7d, Supplementary Discussion), and found that a large cavity within DISP1-A containing the three Na^+ ions is substantially disrupted in DISP1-A-NNN by a series of side-chain rotamer swaps, including interactions across the pseudodyad axis between the altered residues D571N and D1049N, with concomitant straightening and movement of TM4 and TM10 towards each other (Fig. 3c, Extended Data Fig. 7d, bottom, Supplementary Discussion). These movements, associated with Na^+ loss in DISP1-A-NNN, bring into closer proximity the pseudodyad halves of the transmembrane domain (TM1–TM6 and TM7–TM12), suggesting possible modes of allosteric communication from the nexus of Na^+ coordination outward towards ECD1, ECD2 and other Hedgehog-interacting regions of DISP1.

Structure of a ShhN–DISP1-A complex

We determined the structure of DISP1-A in complex with ShhN, a truncated Shh containing residues 26–189 and lacking lipid modifications (2.7 Å overall resolution) (Extended Data Figs. 4, 6, 9, Extended Data Table 1). The largest of the two major density classes contained substantial additional density corresponding to ShhN perched near the top front side of DISP1-A, between ECD1 and ECD2 (Fig. 4a). In the model of this ShhN–DISP1-A complex (Fig. 4b), the ShhN portion of the map resolved residues 39–189, as well as the previously described Zn2+ ion[30] and the di-atomic Ca^{2+} cluster[31], along with all major secondary structure elements and most side chains (Fig. 4a, b, Extended Data Figs. 6, 9).

In the complex, ECD1 and ECD2 of DISP1-A bind ShhN in a pincer-like grasp (Fig. 4a, b), including hydrophobic contacts and possible ionic interactions with total buried surface area of 989.3 Å2 (−8.6 kcal $mole^{-1}$; Methods). The position of ShhN relative to DISP1-A in our complex structure is distinct from the position recently proposed by Cannac et al. 24 for Drosophila Hedgehog (Extended Data Fig. 9c). Notably, the furin-cleaved front-side linker of DISP1-A, which is considerably sharper than in the DISP1-A apo structure, extends from ECD2 upwards and around ShhN in a one-armed molecular embrace (Fig. 4a, b). We extended the model of this linker by an additional 13 residues preceding the furin cleavage site (Extended Data Fig. 2). Improved ECD resolution in the ShhN–DISP1-A map also enabled us to extend the DISP1-A model by an additional 11 residues (399–409) in distal ECD1 (Fig. 4b, Extended Data Fig. 2), revealing a hydrophobic cavity that could interact with an extended hydrophobic moiety (Extended Data Fig. 6f), and reminiscent of the hydrophobic cavity at distal ECD2 (Fig. 1c, Extended Data Fig. 6g).

Conformational dynamics of DISP1

We applied 3DVA23 to this dataset and found the first principal component (PC1) to be anchored at opposite ends by DISP1-A molecules either complexed with or lacking the ShhN ligand (Extended Data Fig. 10a, Supplementary Video 4). A similar range of DISP1-A conformations is found within PC1 of 3DVA of the DISP1-A apoprotein dataset (Extended Data Fig. 10b), suggesting that ShhN binds preferentially to a restricted subset of common DISP1-A conformations.

Close examination revealed that Na+ sites are differentially occupied at opposite extremes of the PC1 reaction coordinates for datasets with or without ShhN (Extended Data Fig. 10a, Supplementary Video 4), with densities corresponding to all three Na^+ ions present at the end anchored by unbound DISP1-A, and only Na^+ site I occupied at the opposite end, anchored by the ShhN-bound complex. Na^+ occupancy thus drives, or is permissive of, alternative conformational states of DISP1, suggesting that chemiosmotically driven flux through the DISP1 transmembrane tunnel could induce conformational changes that cause Hedgehog release after initial binding.

Membrane extraction of Hedgehog lipid adducts

The release of mature Hedgehog signal requires extraction of its covalently linked cholesteryl and palmitoyl adducts from the membrane; thus, the lifted sterol on the front

side of DISP1-A (Fig. 1c) may correspond to an intermediate state of the cholesteryl adduct as it is being removed from its hydrophobic environment. The hydrophobic cavities at the distal tips of ECD1 and ECD2 (Extended Data Fig. 6f, g) are large enough to accommodate the covalently linked Hedgehog lipid adducts, suggesting that they may act as waystations for the ShhNp lipid adducts after membrane extraction and before complex formation with SCUBE2.

Discussion

We propose that DISP1-A extraction and release of the lipid-modified Hedgehog signal proceeds via a state activated for recruitment of SCUBE2 (Fig. 4c). We suggest that activation by DISP1-A binding to Shh at a location approximately 25 Å above the membrane aids in extraction of the ShhNp-linked lipids, and the lifted sterol at the front side of DISP1-A may represent an intermediate in cholesteryl adduct extraction (Fig. 1c). Three prominent features characterize this activated state: (1) a pincer-like action of the split ECDs; (2) a molecular embrace of Shh by the furin-cleaved linker arm; and (3) the possible accommodation of lipid adducts in distal ECD1 and ECD2. This activated state is correlated with loss of Na^+ from sites II and III (3DVA, ShhN-bound state) (Extended Data Fig. 10, Supplementary Video 4), followed by Na^+ flux down its chemiosmotic gradient to re-occupy sites II and III and cause release of ShhNp to SCUBE2—a process incorporating opening of the ECD pincers, expulsion of the ECD1 and ECD2 lipid adducts and withdrawal of the linker embrace, followed by resetting to permit another cycle.

We note from structure-based alignment that each of 15 protein-derived Na^+-liganding oxygens in DISP1 (10 from side-chains, 5 from main-chain carbonyls) is conserved in PTCH1, as are the three charge-neutralizing intramembrane acidic residues (Extended Data Fig. 11). This degree of conservation exceeds that of the overall protein sequence (19% identity overall), and strongly supports the functional role of Na^+ flux in PTCH1 suppression of SMO activity, consistent with a previous demonstration of PTCH1 dependence on a transmembrane Na^+ gradient for its function[27]. All of these residues are also conserved by sequence alignment in PTCH2, which also functions to suppress SMO[32]. By contrast, DISP2, which does not rescue disp function in Drosophila[6] and probably lacks Hedgehog-releasing activity, has only one of three charge-neutralizing intramembrane acidic residues and six of ten side-chain oxygens. Prokaryotic RND transporters harbour distinct residues at these Na^+-coordinating sites (Extended Data Fig. 11), but most retain interactions between TM4 and TM10 that are conditional on cation binding, pointing to a common mechanism for harnessing chemiosmotic gradients (Supplementary Discussion).

How do DISP1 and PTCH1 produce such distinct functional effects on Hedgehog-pathway activation? Our analysis suggests the use of chemiosmotic force from the metazoan transmembrane Na^+ gradient to power the release of lipids from membranes. For PTCH1, cholesterol removal via an enclosed sterol conduit in the PTCH1 ECD regulates SMO by depriving it of sterol that must be bound within the interior of its seven-transmembrane helix bundle for activity[33,34]. DISP1 also appears to extract lipids from the membrane, but these lipids are covalently attached to the Hedgehog protein signal, necessitating a split of the DISP1 ECD to accommodate the protein moiety. Evolutionary acquisition of the furin

cleavage site that permits this split, and of the linker arm that contacts ShhNp, apparently occurred by insertion into the Disp1 gene of a single small exon that encodes both features (Extended Data Fig. 2). A fundamental mechanistic similarity is indicated by a lifted sterol in both DISP1 and PTCH1, at corresponding positions within the 12-transmembrane helix bundle35. The unusual positions of these sterols at corresponding locations in both proteins suggest partial extraction from the membrane, perhaps representing a common intermediate in the lipid extraction activities of both proteins.

Methods

No statistical methods were used to predetermine sample size. All proteins, including DISP1 variants, ShhN, ShhNp and SCUBE2, were of mouse origin (Mus musculus). Cell lines were not tested for mycoplasma contamination. All cell lines grew normally.

DISP1 expression and purification

All constructs were cloned using Gibson Assembly. In DISP1-A, DISP1-A-NNN and the ion-site mutants, amino acids 3 to 171 were deleted from the full-length (1–1521) DISP1. For protein expression, DISP1-A–ShhNp binding assays and ShhNp release assays, different DISP1 variants were cloned into the pcDNA3.1 vector[1]. For detection of protein expression levels in Extended Data Fig. 1d, HEK 293T cells (ATCC, CRL-3216) were seeded into a six-well plate. Plasmids encoding DISP1 or DISP1-A with the SBP and HA tags at the C terminus were transiently transfected into the cells using Lipofectamine 3000 (ThermoFisher). Two days after transfection, the cells were lysed and incubated for 1 h at 4 °C in buffer containing 20 mM HEPES pH 7.5 (Teknova), 300 mM NaCl (Teknova), 2 mg ml−1 iodoacetamide (Sigma), 1% n-dodecyl-β-d-maltoside (DDM) (Anatrace), 0.2% CHS (Anatrace) supplemented with protease inhibitors (ThermoFisher). Protein extracts were cleared by a subsequent centrifugation (100,000g, 30 min, 4 °C). Western blotting was performed using Criterion TGX stain-Free precast gels (Bio-Rad) and Immobilon-P PVDF membrane (Millipore). PVDF membranes were immunoblotted overnight at 4 °C with anti-HA rabbit polyclonal (1:1,000, Cell Signaling) or anti-β-actin rabbit polyclonal (1:1,000, Cell Signaling) antibodies followed by a 1-h incubation with the corresponding horseradish peroxidase-conjugated secondary antibodies (1:2,000, Promega) at room temperature. The blots were developed using SuperSignal West Pico PLUS substrate (ThermoFisher).

For large-scale protein purification, C-terminally streptavidin-binding peptide (SBP)-tagged DISP1-A was cloned into a BacMam expression vector, PVLAD6. Baculoviruses were produced in Sf9 cells (ATCC, CRL-1711) as previously described[1,27]. HEK 293F cells (ThermoFisher, R79007) were cultured in suspension using Free-Style medium (ThermoFisher) until the density reached 1.5–2 × 10^6 cells per ml, and cells were transduced with DISP1-A-SBP baculoviruses in the presence of 10 mM sodium butyrate (Sigma). Forty-eight hours after transfection, cells were collected and stored at −80 °C. For DISP1-A-NNN, plasmids encoding DISP1-A-NNN-SBP were transfected into the HEK 293F cells using linear polyethylenimines (Polysciences). Both DISP1-A and DISP1-A-NNN were purified essentially as previously described1. Cells were disrupted using a hypotonic buffer (20 mM HEPES pH 7.5, 10 mM $MgCl_2$ (Teknova), 10 mM KCl (Teknova), 0.25 M

sucrose (Sigma)) in the presence of benzonase (Sigma) and protease inhibitors. Following centrifugation (100,000g, 30 min, 4 °C), the pellets were solubilized using a glass Dounce tissue homogenizer in lysis buffer (20 mM HEPES pH 7.5, 300 mM NaCl, 2 mg ml−1 iodoacetamide, 1% DDM, 0.2% CHS) supplemented with protease inhibitors. The sample was incubated for 2 h at 4 °C with gentle rotation, then centrifuged (100,000g, 30 min, 4 °C) for collection of the supernatant. The C-terminally SBP-tagged DISP1-A or DISP1-A-NNN was captured using streptavidin–agarose affinity resin (ThermoFisher). After a 3-h incubation period at 4 °C, the resin was packed into a disposable column by gravity flow. The resin was first washed with 30 column volumes (CVs) of wash buffer (buffer W, 20 mM HEPES pH 7.5 and 300 mM NaCl) containing 0.03% DDM, 0.006% CHS; then with 30 CVs of buffer W containing 0.12% LMNG (Anatrace), 0.024% CHS and 0.025% GDN (Anatrace) to exchange detergents; and finally with 30 CVs of buffer W containing 0.012% LMNG, 0.0024% CHS and 0.0025% GDN. Protein was eluted in buffer W containing 0.012% LMNG, 0.0024% CHS, 0.0025% GDN and 2.5 mM biotin (Sigma). The eluted protein was concentrated with an Amicon Ultra filter (100 kDa cut-off, Millipore) and loaded onto a Superose 6 Increase 10/300 GL column (GE Healthcare) in buffer W containing 0.012% LMNG, 0.0024% CHS and 0.0025% GDN plus 5 mM $CaCl_2$ (Sigma).

ShhN expression and purification

A DNA fragment encoding mouse ShhN residues 26–189 was cloned into a pHTSHP vector with N-terminal His8 tags[31]. Protein was expressed in Escherichia coli strain BL21(DE3) and purified as previously described[1]. The cell lysate was first centrifuged at 8,000g for 15 min (4 °C), then the filtered supernatant was applied to the Ni-NTA resin. After elution from the Ni-NTA column, the N-terminal tags were cleaved with HRV3C protease. The protein was dialysed against 20 mM HEPES, 100 mM NaCl and 7 mM β-mercaptoethanol, and further purified by SP sepharose cation-exchange chromatography.

SCUBE2 expression and purification

Mouse SCUBE2 lacking amino acids 30–281 (to mimic the effect of furin cleavage at an internal site) was 3×Flag-tagged at the C terminus and expressed in Flp-In T-REx 293 cells (ThermoFisher, R78007), as previously described[20]. Cultures were induced with doxycycline and transitioned to serum-free medium (DMEM (ThermoFisher) supplemented with 1x insulin–transferrin–selenium (ThermoFisher), 10 mM HEPES, 1× GlutaMAX and 5 μg ml−1 doxycycline). After 3–4 days, SCUBE2-conditioned medium was collected and clarified by centrifugation and membrane filtration. After concentrating by ultrafiltration (Vivaflow 200/30 kDa, Sartorius), SCUBE2 was purified by heparin and anti-Flag M2 affinity chromatography. Eluted protein was concentrated to 9.13 mg ml−1 by ultrafiltration (Amicon Ultra 30 kDa, Millipore). The eluting 3×Flag peptide was washed out during the final concentration step.

Cryo-EM sample preparation and data acquisition

For DISP1-A, 2.5 μl of purified and concentrated sample at a concentration of 1.56 mg ml^{-1} was applied to glow-discharged gold grids covered with holey carbon film (Quantifoil, 300 mesh 1.2/1.3) and plunge frozen using a Vitrobot Mark IV, with blotting time of 4 s and blotting force 0, at 8 °C and 100% humidity. DISP1-A-NNN cryo-EM grids were prepared similarly, but using gold-grids covered by a holey gold film (Quantifoil UltrAufoil, 300 mesh 1.2/1.3) and a sample concentration of 0.3 mg ml^{-1}. For ShhN–DISP1-A complex, purified DISP1-A was incubated with ShhN at a 2.7:1 molar ratio (27 μM ShhN, 10 μM DISP1-A) for 3 h (4 °C) before cryo-sample preparation. DISP1-A–ShhN grids were prepared in the same way as that for DISP1-A.

Cryo-EM data for DISP1-A and ShhN–DISP1-A were collected with a Titan Krios microscope operated at 300 keV and equipped with a Bio Quantum post-column energy filter with zero-loss energy selection slit set to 20 eV. Using SerialEM37, images were recorded automatically at a nominal magnification of 105,000× (true magnification 59,880×), with defocus range set to −0.5 to −1.5 μm. Images were recorded with a post-GIF Gatan K3 camera in super-resolution single-electron counting mode with a calibrated pixel size of 0.4175 Å (physical pixel size of 0.835 Å). The DISP1-A-NNN samples were imaged on a different Titan Krios with identical parameters, but a slightly different calibrated pixel size of 0.417 Å. Data collection statistics are shown in Extended Data Table 1.

Image processing and map calculation

As part of an on-the-fly image-processing pipeline, which processes micrographs immediately after acquisition, we used MotionCor2[38] to correct motion of each dose fractionated movie stack, sum motion-corrected frames with and without dose weighting, and bin images in Fourier space to the physical pixel size (~0.835 Å) for further image processing. Motion-corrected, dose-weighted sums were used for contrast transfer function determination and resolution estimation in cryoSPARC[39]. Particles were picked in cryoSPARC first using a Gaussian template, and then re-picked with low-resolution templates generated from an initial structure. Subsequent image processing was carried out in RELION[40] and cryoSPARC. The flow chart of image processing is illustrated in Extended Data Fig. 3 (DISP1-A and DISP1-A-NNN) and Extended Data Fig. 9 (ShhN–DISP1-A). Conversion of data from cryoSPARC to RELION was performed using UCSF pyem[41]. Directional Fourier shell correlation curves were determined as previously described[42].

3DVA23 of DISP1-A alone was conducted based on the early non-uniform refinement shown in Extended Data Fig. 3 (2.4 Å nominal resolution, 974,614 particles), using a five-component decomposition solved over 40 iterations. During 3DVA, the data were filtered by an 8th-order Butterworth high-pass filter with a cut-off frequency of 40 Å and a 1.5-order Butterworth low-pass filter with a cut-off frequency of 3.5 Å, as well as a soft mask containing the entire protein but excluding the detergent micelle. Trajectories representing each variability component were computed using ‘simple’ mode (that is, each step is calculated by weighted addition of variability component maps to the mean structure) with 20 frames and no filters. 3DVA of ShhN–DISP1-A was performed similarly, based

on non-uniform refinement of all apo and complex particles combined (2.7 Å nominal resolution, 356,610 particles), but with no high-pass filter owing to the need to capture the appearance and disappearance of ShhN.

Model building and refinement

The de novo atomic models of DISP1-A were built in Coot[43], refined in PHENIX[44] and finalized in ISOLDE[45]. Starting from a predicted model from PHYRE2[46] and a combined density of R and T conformers, we manually fitted transmembrane helices into the corresponding density and then traced the backbone of ECDs and linkers in between those transmembrane helices in Coot. The preliminary model was then mutated based on Mouse DISP1 sequence and refined using real space refinement in PHENIX. Based on residual unmodelled density near the protein, ligands were added and refined in real space using Coot and PHENIX, respectively. Starting from this 'common model' built referring to the combined density of R and T, we obtained models for each conformer (R, T and NNN) by refining this 'common model' against the final density of each conformer individually, removing atoms unresolved in each density and then finalizing the models with ISOLDE (largely to improve steric clashes). The ShhN–DISP1-A complex was treated in the same manner, but using several crystal structures of mammalian Shh as initial models (Protein Data Bank (PDB) IDs: 1VHH, 4C4N and 6PJV). All models were validated by wwPDB validation server47 and no major issues were reported in our three models.

Visualizations of the atomic models (figures and videos) were made using UCSF Chimera48, ChimeraX[49] and PyMOL (The PyMOL Molecular Graphics System, Version 2.0 Schrödinger, LLC.). The ion conduction path was mapped using Caver 3[29] and ion coordination geometries were analysed with the CheckMyMetal web server[26]. DISP1–AShhN interaction interface area and the solvation free-energy gain upon the formation of the interfaces were calculated using PISA[50]. Clustal Omega[51] and the ESPript server[52] was used in preparation of the protein sequence alignment (Extended Data Fig. 2).

Rapid, quantitative ShhNp release rate assay

Disp$^{-/-}$ mouse embryonic fibroblasts (MEFs)[6,20], were cultured on 24-well plates in DMEM supplemented with 10 % FBS and 1% penicillin-streptomycin-glutamine (ThermoFisher). DISP1–mEGFP variants were transfected into the cells along with a NanoLuc–Shh fusion in which the nanoluciferase coding sequence was inserted between E131 and D132 in Shh. The mass ratio of plasmids expressing DISP1 variants and NanoLuc–ShhNp was 1 to 2. An EGFP expression construct was used as a negative control for conditions lacking DISP1 variants. Two days after transfection, following a quick wash with DMEM, cells were incubated with cycloheximide (100 μg ml^{-1}, Sigma) in DMEM for 50 min. Cells were then incubated in the desired medium either with or without SCUBE2 protein (1 μM (Fig. 2b) or 150 nM (Fig. 2c)) at 37 °C with gentle shaking (125 rpm). Small aliquots of supernatant were removed sequentially at multiple time points, and collected supernatants were cleared by a centrifugation at 3,000g for 30 min at 4 °C. NanoLuc-ShhNp luminescence level was measured using Nano-Glo Luciferase Assay System (Promega), following the manufacturer's protocol, and the measured luminescence was corrected to

account for the decreased supernatant volume through time. At the end of the experiment, cells were washed with PBS and lysed with the passive lysis buffer (Promega). Released NanoLuc–ShhNp luminescence at each time point was normalized to the GFP level, the total protein in cell lysates (measured using Pierce BCA protein assay kit, ThermoFisher), and to the total luminescence of ShhNp (luminescence level in cell lysates plus total NanoLuc–ShhNp released into supernatant by the final time point). The linear portion of the release curves was used to calculate the ShhNp release rate. ShhNp release endpoint assay Disp$^{-/-}$ MEFs[6,20], were cultured on six-well plates in DMEM supplemented with 10 % FBS and 1% penicillin-streptomycin-glutamine. All cell transfections were performed using Lipofectamine 3000. Plasmids encoding DISP1 variants were transfected into the cells along with full-length Shh constructs. The ratio of plasmids expressing DISP1 variants to Shh was 1 to 2. For conditions that did not have DISP1 variants or Shh, a GFP construct was used as a negative control to replace the missing partner. Two days after transfection, following a quick wash with DMEM, the cells were shifted to SCUBE2(Δ30–281) (mouse SCUBE2, with an N-terminal truncation)-conditioned medium or control medium (600 µl per well). After 16 h of incubation, the medium was collected and centrifuged at 18,000g for 30 min (4 °C). The supernatant was probed by immunoblotting for ShhNp (anti-Shh rabbit monoclonal, 1:1,000, Cell Signaling), 3×Flag-tagged SCUBE2 (anti-Flag m2 mouse monoclonal, 1:1,000; Sigma). Cells were lysed using a buffer containing 20 mM HEPES pH 7.5, 300 mM NaCl, 2 mg ml^{-1} iodoacetamide, 1% DDM, 0.2% CHS supplemented with protease inhibitors (400 µl per well, 1 h at 4 °C). After a centrifugation of 100,000g for 30 min at 4 °C, cell lysate was probed by immunoblotting for ShhNp (anti-Shh rabbit monoclonal, 1:1,000), DISP1–HA or DISP1–mEGFP (anti-HA rabbit polyclonal, 1:1,000 or anti-GFP rabbit polyclonal, 1:2,000, Invitrogen), and β-actin (rabbit polyclonal, 1:1,000). SCUBE2-conditioned medium was prepared in the same way as described above in SCUBE2 expression and purification. Control medium was prepared as for SCUBE2-conditioned medium but without doxycycline induction.

DISP1-ShhNp co-immunoprecipitation

The DISP1-ShhNp binding assay (Extended Data Fig. 8f) was conducted using the HEK 293 Flp-In T-REX ShhNp-producing cell line[20]. ShhNp-producing cells were maintained in DMEM with 10% FBS and 1% penicillin-streptomycin-glutamine. Plasmids of C-terminally SBP and HA-tagged DISP1-A variants were transiently transfected into the cells using Lipofectamine 3000. One day after transfection, full-length Shh expression was induced by 5 µg ml^{-1} Doxycycline (Sigma) in DMEM F-12 (ThermoFisher) supplemented with 1% insulin-transferrin–selenium and 1% penicillin-streptomycin-glutamine. Another day after ShhNp expression was induced, cells were lysed and incubated for 1 h at 4 °C in the same buffer as that in ShhNp release endpoint assay. Following a subsequent centrifugation (100,000g, 30 min, 4 °C), Streptavidin-agarose affinity resin was used to pull down theSBP-tagged DISP1-A variants, together with any bound ShhNp, from the supernatant. After a 2-h incubation period at 4 °C, the resin was washed with buffer W containing 0.03% DDM and 0.006% CHS. Protein was eluted in the same buffer supplemented with 2.5 mM biotin. Immunoprecipitates were analysed by Western blot as described above using the following

antibodies: anti-HA rabbit polyclonal (1:1,000), anti-Shh rabbit monoclonal (1:1,000) and anti-β-actin rabbit polyclonal (1:1,000).

Reporting summary

Further information on research design is available in the Nature Research Reporting Summary linked to this paper.

Extended Data

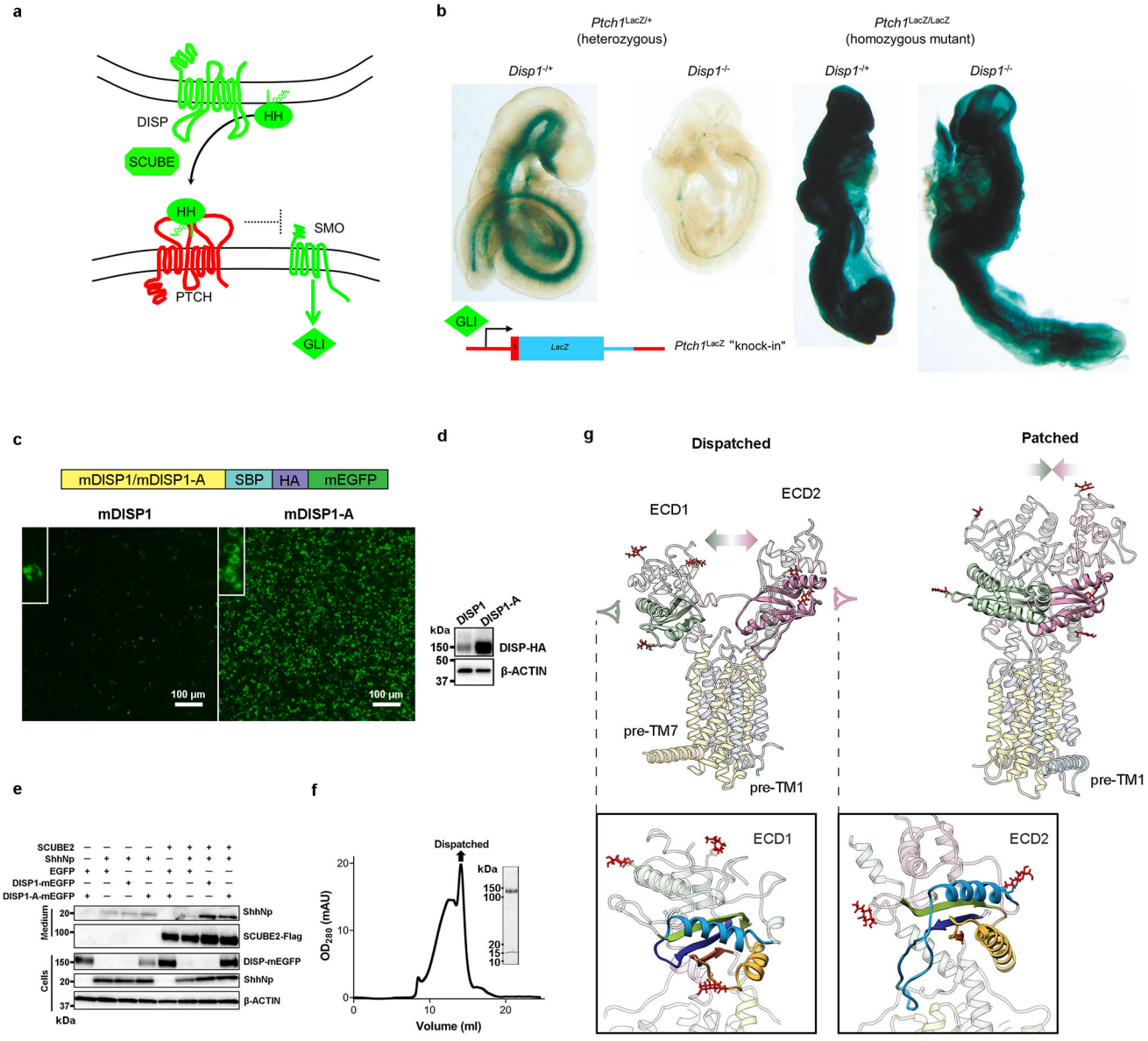

Extended Data Fig. 1 |. Structurally related transporters Dispatched and Patched in Hedgehog signalling.

a, b, Opposing functions of Dispatched and Patched in Hedgehog signalling. **a**, The HH protein signal, covalently modified by cholesterol and palmitate, requires the action

of DISP1 and SCUBE for release from the membrane of producing cells. HH then uses its palmitoyl adduct to clog the sterol transport conduit and block the function of its receptor PTCH1 in responding cells. The loss of PTCH1 sterol transport activity permits accumulation of cholesterol within the inner leaflet to levels that activate SMO by binding within its seven transmembrane helix bundle, resulting in activation of the GLI transcriptional effector of Hedgehog signalling. **b**, As *Ptch1* is a target for GLI activation, the X-Gal staining of a $Ptch1^{LacZ}$ knock-in allele[53] provides an indication of Hedgehog pathway activity (leftmost embryo). Homozygous mutation of *Disp1*[6–10] causes a loss of nearly all embryonic Hedgehog pathway activity (2nd embryo from left)[54], whereas homozygous disruption of *Ptch1* leads to unregulated ectopic pathway activity, regardless of the functional status of *Disp1* (rightmost two embryos)[53]. **c–f**, Truncated DISP1 protein. As murine full-length DISP1 protein was poorly expressed in HEK293 cells, we tested a variety of constructs, and ultimately settled on an N-terminal truncation. Although its export activity was partially reduced, truncated DISP1-A protein nevertheless mediated efficient release of ShhNp (autoprocessed, lipid-modified Shh protein) into cell culture medium containing SCUBE2 (mouse SCUBE2, lacking amino acids 30–281) upon transfection into $Disp^{-/-}$ mouse embryonic fibroblasts6,20 (MEFs), indicating preservation of its function. **c**, DISP1-mEGFP and DISP1-A-mEGFP in HEK293T cells with magnified insets showing expression on the cell membrane. **d**, Western blot showing high level of DISP1-A expression relative to DISP1 (both proteins were SBP and HA-tagged at the C-terminus). **e**, Functional assay (Methods, ShhNp release endpoint assay) in $Disp^{-/-}$ MEFs. Culture media and cell lysates from transiently transfected $Disp^{-/-}$ MEFs were probed by immunoblotting for expression of DISP-mEGFP (SBP, HA and mEGFP tagged at the C-terminus, see panel **c**), ShhNp, and SCUBE2. DISP1 and DISP1-A both released ShhNp in the presence of SCUBE2. β-ACTIN, loading control. **f**, Size exclusion chromatography of purified DISP1-A, together with the SDS-PAGE of the indicated fraction, corresponding to monomeric DISP1-A. Panels **c–f**, show representative results (n = 4 biologically independent replicates). **g**, Structural comparison between DISP1-A and mouse PTCH155 (PDB ID: 7K65). The ECDs, closely apposed in PTCH1 to form a conduit for sterol transport, in DISP1-A are splayed apart. Conserved ferredoxin-like α + β open-faced sandwich folds are highlighted (lime for ECD1 and pink for ECD2). Magnified views in spectral sequence from N to C termini of the α + β open-faced sandwich folds in DISP1-A ECD1 (bottom left) and ECD2 (bottom right). Distal structures inserted into the peripheral loops of the ferredoxin-like folds are structurally unrelated to each other or to distal PTCH1 ECD structures. Red symbols indicate the five N-linked glycosylation sites, three in ECD1 (N362, N390 and N475) and two in ECD2 (N834 and N915), which can be inferred from additional densities that extend from N-X-S/T sequences in the extracellular loops. Panels **d, e, f**, see Supplementary Fig. 1 for gel source data.

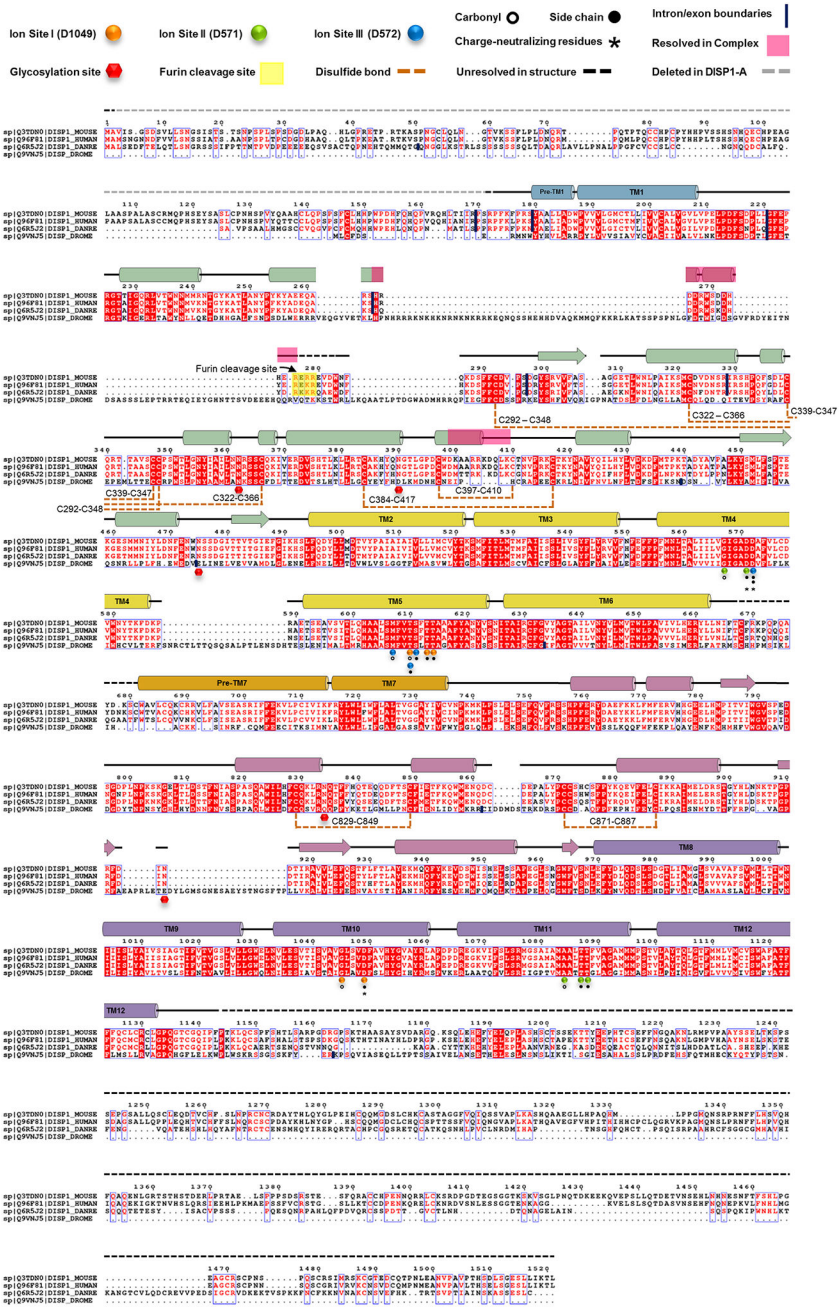

Extended Data Fig. 2 |. Dispatched protein sequence alignment and structural features. Sequence alignment of Dispatched proteins from *Mus musculus* (mouse), *Homo sapiens* (human), *Danio rerio* (zebrafish) and *Drosophila melanogaster* (fruit fly). Secondary structure elements and other features are indicated above the sequence, with subdomains coloured according to Fig. 1a. Protein sequences were aligned using Clustal Omega[51] and the ESPript server[52]. TM, transmembrane helix.

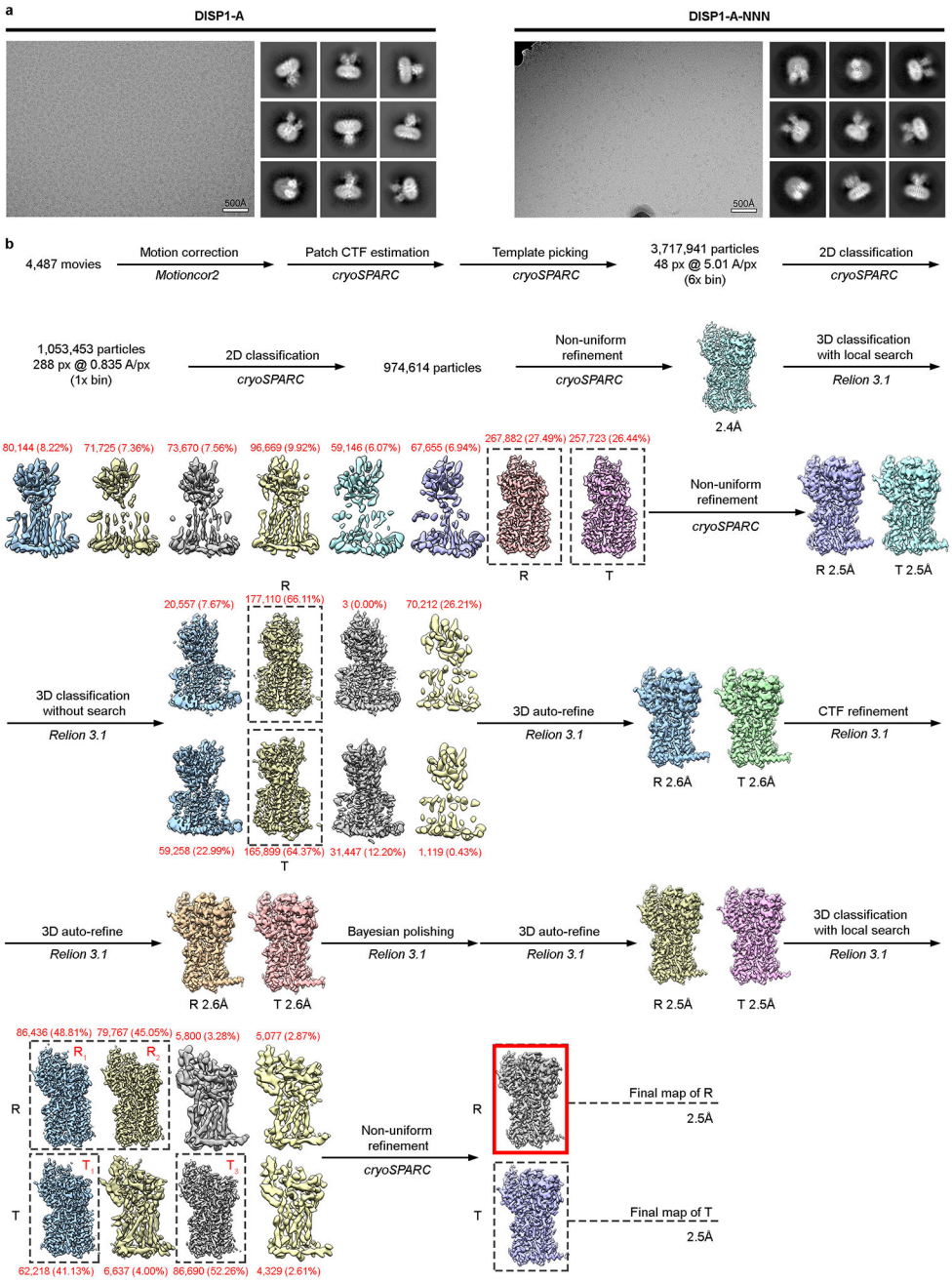

Extended Data Fig. 3 |. Cryo-EM data and image processing flow for DISP1-A and DISP1-A-NNN.

a, A representative cryo-EM micrograph (n = 4487 for DISP1-A, n = 4467 for DISP1-A-NNN) and several highly-populated, reference-free 2D class averages are shown for DISP1-A (left) and DISP1-A-NNN (right). The micrograph for DISP1-A-NNN has been contrast-stretched for display in order to account for the presence of a gold edge in the upper left corner of the image (the DISP1-A-NNN particle distribution on this grid necessitated targeting of the gold edge). **b**, Schematic flow-chart representing the image processing approach for DISP1-A. Thumbnail images of each 3D class or refinement are shown along with global GS-FSC resolution in black, particle counts in red, and dashed black boxes to

indicate selected 3D classes. After separation of the R and T conformations in the first round of 3D classification, the identical processing flows for the two conformations are shown in parallel. Cryo-EM map (Red box) and atomic model of R conformation are used in main figures to present DISP1-A features. Subclasses of R and T conformations, R_1, R_2, T_1 and T_3, are labeled.

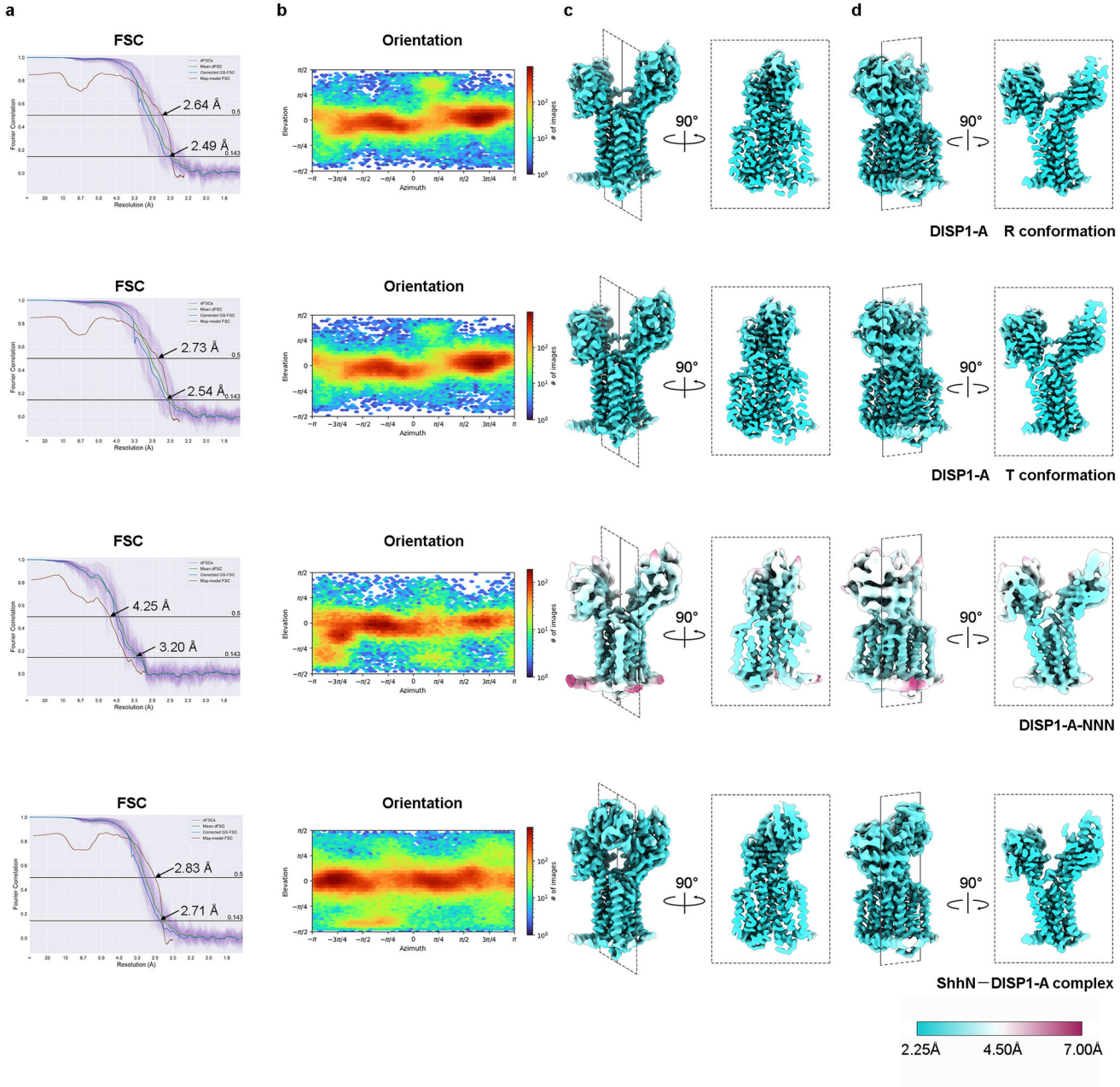

Extended Data Fig. 4 |. Cryo-EM density and atomic model quality.

Fourier shell correlation curves (**a**), particle orientation distributions (**b**), and local resolution maps (**c, d**) are shown for R and T conformations of DISP1-A, DISP1-A-NNN, and for ShhN–DISP1-A complex. The ‘gold-standard’ independent half-map FSC curves and

orientation distributions were determined during refinement in cryoSPARC, map-to-model FSC curves were calculated in PHENIX using protein chains only, and directional FSC curves were estimated as in ref.[42]. The orientation distributions are plotted such that an elevation angle of 0° corresponds to a 'side-view' perpendicular to the transmembrane helices; in each case the predominant views are 'side-views' at a wide range of azimuthal angles. Local resolution estimates were computed using the BLOCRES algorithm as implemented in cryoSPARC.

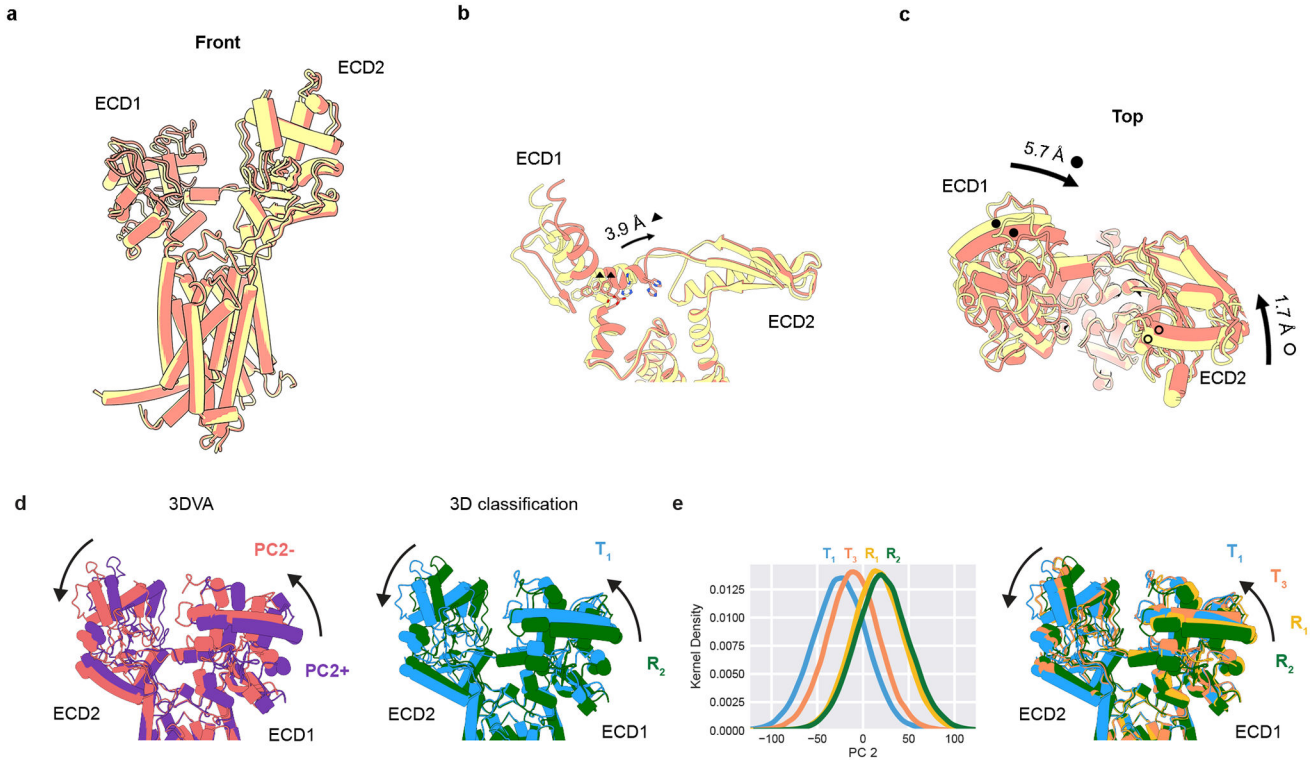

Extended Data Fig. 5 |. Coincident modes of DISP1 conformational flexibility revealed by 3D classification and 3D variability analysis (3DVA).

a, Overlay comparing front view of R and T conformations (khaki and salmon, respectively) from 3D classification. Major conformational changes are localized to the extracellular domains. **b**, Cut-away view showing the formation of a 'kink' in the back-side linker of the T conformation, with an accompanying shift of about one helix turn that breaks a hydrogen bond between linker residue H777 and the backbone carbonyl of K767. **c**, Extracellular view of the R and T conformations, highlighting the movement of secondary structure elements in ECD1 (> 5 Å) and ECD2 (~2 Å). The shift of ECD1 and the formation of the inter-ECD linker 'kink' appear intimately related. Numbers indicate distances (Å) between the Cα of F772 in R and T (marked by ▲ in **b**) and R382 and S898 (marked by ● and ○, respectively, in **c**). **d**, Comparison of the most extreme R and T conformations from 3D classification (right) and the two extreme ends of PC2, PC2+ (R-like) and PC2- (T-like), from 3DVA left) shows that a nearly identical mode of motion is captured by both techniques. **e**, Distributions of DISP1-A particles stratified by their 3D class along the PC2 axis of 3DVA, demonstrating colinearity between the 3DVA trajectory and the 3D subclasses ordered by

apparent conformation. T_1 and T_3, and R_1 and R_2, respectively, are subclasses of T and R conformations resolved by 3D classification (Extended Data Fig. 3).

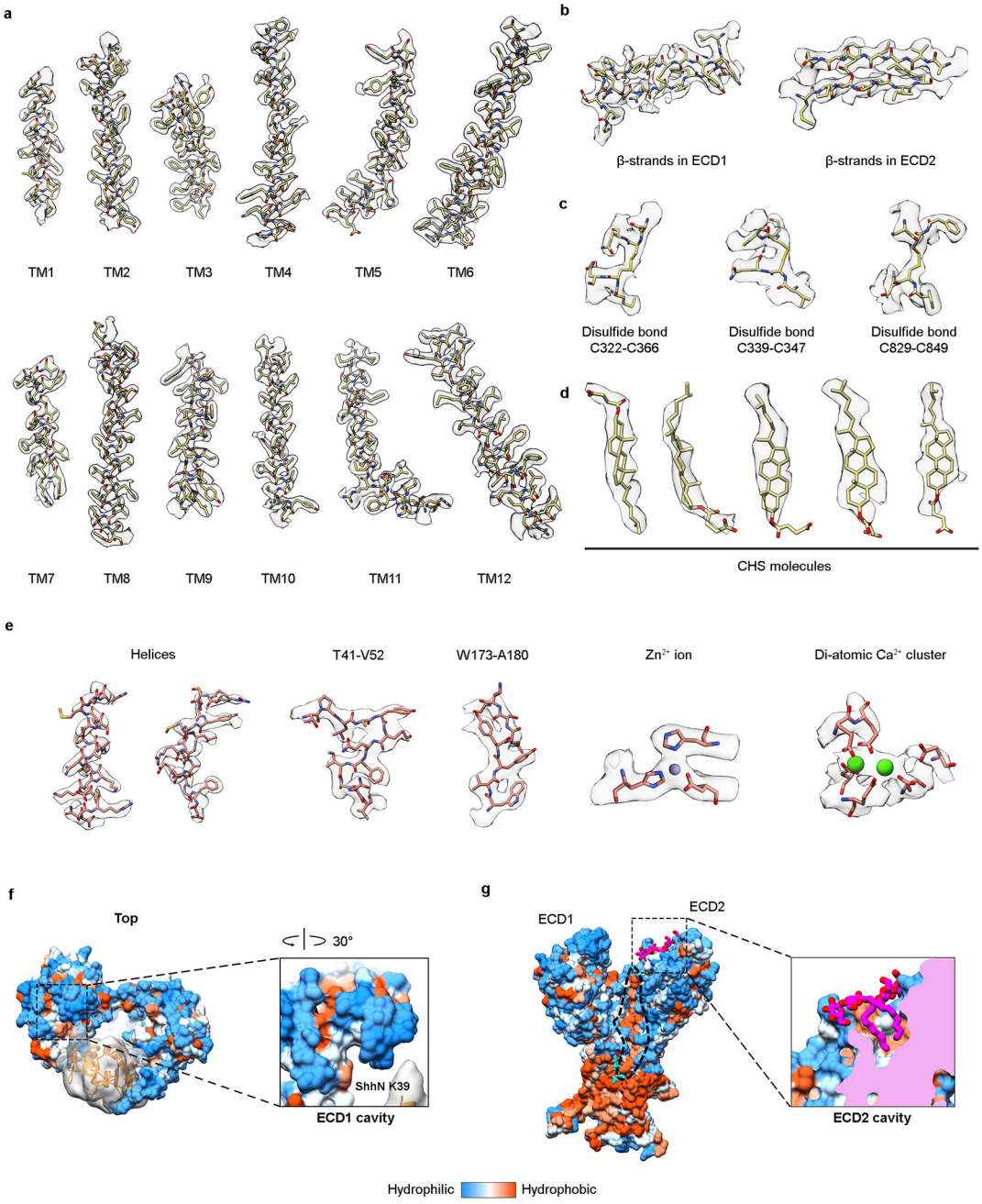

Extended Data Fig. 6 |. Representative cryo-EM densities from selected structural features. **a–d**, Representative cryo-EM densities from 3D reconstruction of DISP1-A, conformation R. a, Densities of all transmembrane helices. **b**, Representative densities of beta-sheets from ECD1 and ECD2. **c**, Cryo-EM densities of three representative disulfide bonds. **d**, Cryo-EM densities of five representative CHS molecules. **e**, Representative cryo-EM densities in ShhN from 3D reconstruction of ShhN–DISP1-A complex. **f, g**, Representation of surface

hydrophobicity, viewed from top (**f**, left) or a top-front position of DISP1-A (**g**, left). Close-up views of hydrophobic cavities in both ECD1 (**f**, right) and ECD2 (**g**, right). A hydrophobic track beginning near the front-side lifted sterol (cyan) extends outward from the membrane (dotted shape). The enclosed hydrophobic conduit employed by the PTCH1 protein for sterol movement away from the membrane is formed by the juxtaposition of ECD1 and ECD2. In DISP1, although ECD1 and ECD2 are split apart in a manner that would bisect this conduit, the ECD2 portion retains a series of hydrophobic residues that line its inner surface, which could perhaps form a partial hydrophobic conduit to the hydrophobic cavities near the distal tips of ECD1 and ECD2, analogous to the sterol conduit within the center of the conjoined ECDs of PTCH1.

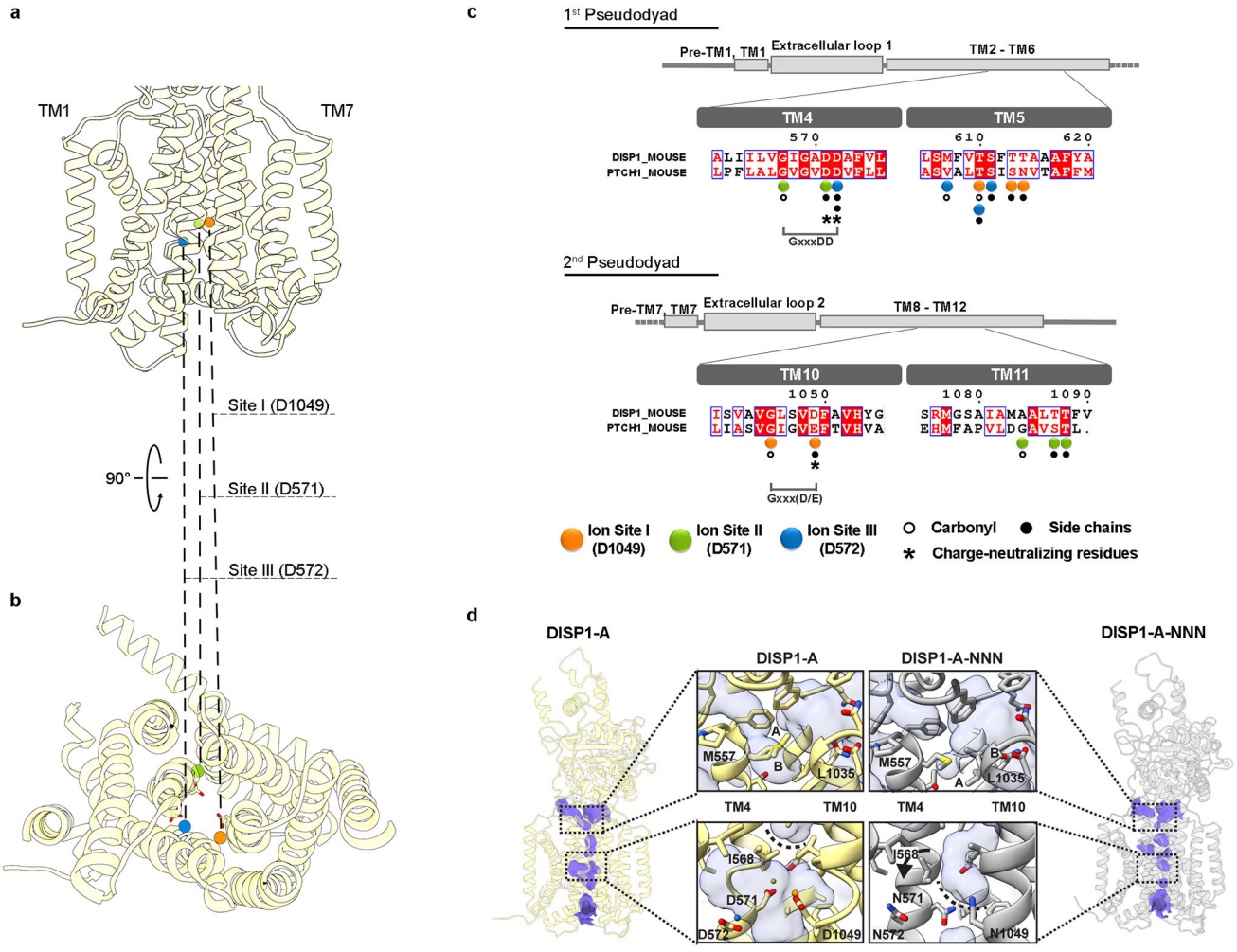

Extended Data Fig. 7 |. Na+-coordinating amino acid residues in DISP1, and conformational rearrangements within the transmembrane Na^+ pathway in DISP1-A-NNN.

a, b, Side (**a**) and extracellular (**b**) views of three Na^+ ion binding sites within the transmembrane domain, each labeled with its associated charge-neutralizing intra-membrane Asp. **c**, Residues in DISP1 with carbonyl oxygens or side-chain residues that coordinate Na^+ and carboxylate residues that neutralize Na^+ charge are conserved in PTCH1 (see also Extended Data Fig. 11). **d**, Solvent excluded surfaces (1.4 Å probe radius) reveal

transmembrane cavities within DISP1-A (left) that are altered in DISP1-A-NNN (right). Two extracellular branches (upper insets) that provide access to the central channel can be individually opened or closed depending on alternate conformations of M557 (‘A’ and ‘B’ in DISP1-A) and alternate conformations of L1035 (‘A’ and ‘B’ in DISP1-A-NNN). Significant rearrangements also take place around a mid-membrane water-filled cavity containing the three ion coordination sites (lower insets). In DISP1-A, short kinks in TM4 and TM10 position I568 above this cavity. In DISP1-A-NNN, however, TM4 and TM10 straighten, rotating I568 and D571N and D1049N into this cavity, dramatically reducing its volume and isolating the channel from its intracellular exit (see Supplementary Discussion).

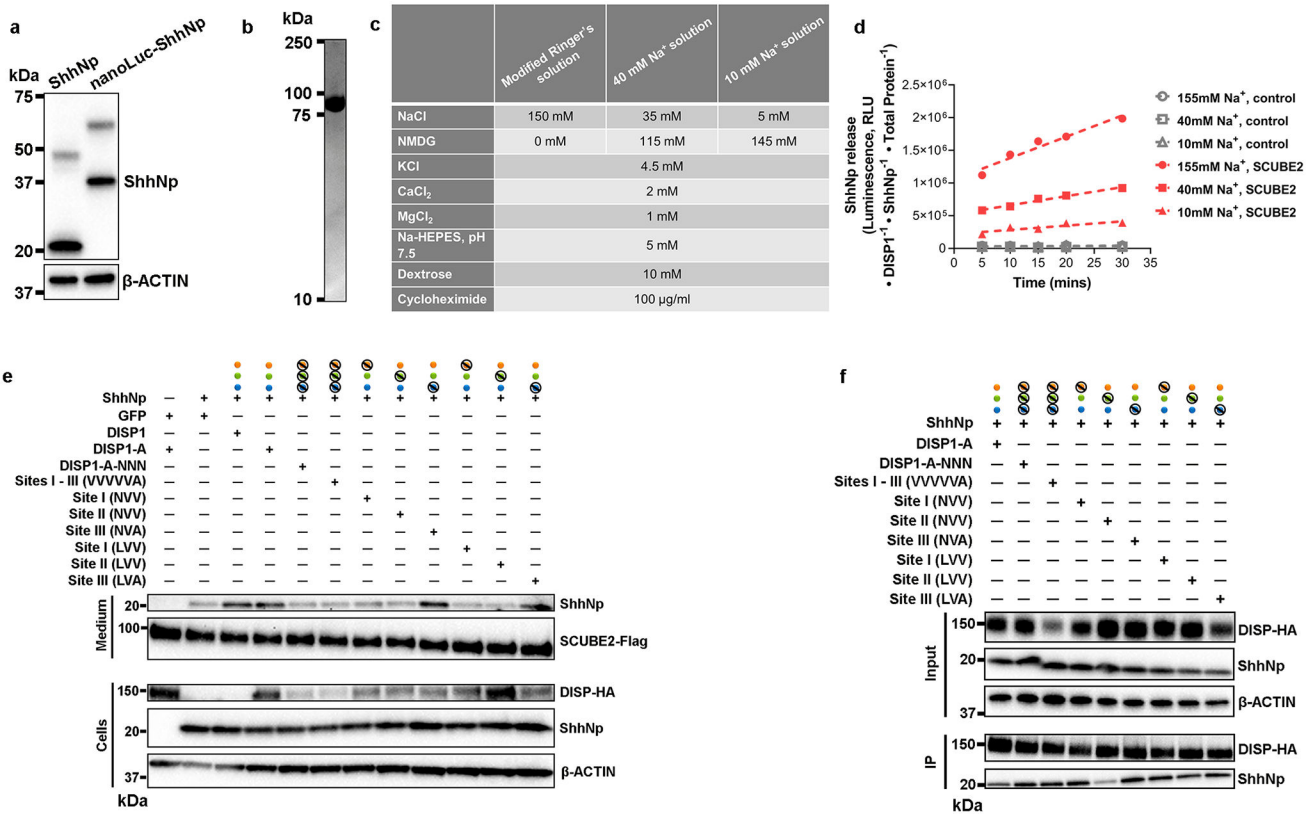

Extended Data Fig. 8 |. Quantitative luciferase-based assay of ShhNp release.

a, Inserting Nanoluciferase coding sequence between E131 and D132 of Shh does not affect Shh autoprocessing and associated lipid modification. Immunoblotting of ShhNp detects both precursor and processed forms of the protein. Most of the expressed nanoluciferase-inserted Shh is in the processed form. **b**, Coomassie blue staining of purified SCUBE2 (Δ30–281) protein. **c**, Composition of buffers used in this study(see Fig. 2b, c). **d**, Time course of NanoLuc-ShhNp release at different Na^+ concentrations (see panel **c**) with or without SCUBE2 (Δ30–281, 1μM). One representative set of normalized data (see Methods) with linear regression (dashed lines) is shown for each condition (n = 4 biologically independent experiments). The release rate determined as the slope of the linear regression line is presented in Fig. 2b. **e**, Western blot-based ShhNp release assay (Methods, ShhNp release endpoint assay). Culture media and cell lysates from transiently transfected $Disp^{-/-}$ MEFs were probed by immunoblotting for DISP

HA (SBP and HA-tagged at the C-terminus), ShhNp, and SCUBE2. β-ACTIN, loading control. **f**, DISP-ShhNp binding assay using HEK293 with stably integrated constructs for doxycycline-inducible expression of full-length Shh20. DISP1-A variants tagged with SBP and HA at the C-terminus (DISP-HA) were immunoprecipitated with Streptavidin resin, and ShhNp detected by Western blot. Alterations in ion site residues as follows: DISP1-A-NNN, D571N/D572N/D1049N; DISP1-A-VVVVVA, T613V/T614V/T1087V/T1088V/T610V/S611A; Site I (NVV), D1049N/T613V/T614V; Site II (NVV), D571N/T1087V/T1088V; Site III (NVA), D572N/T610V/S611A; Site I (LVV), D1049L/T613V/T614V; Site II (LVV), D571L/T1087V/T1088V; Site III (LVA), D572L/T610V/S611A. Panels **a, b, e, f**, show representative results (n = 3 biologically independent replicates, see Supplementary Fig. 1 for gel source data).

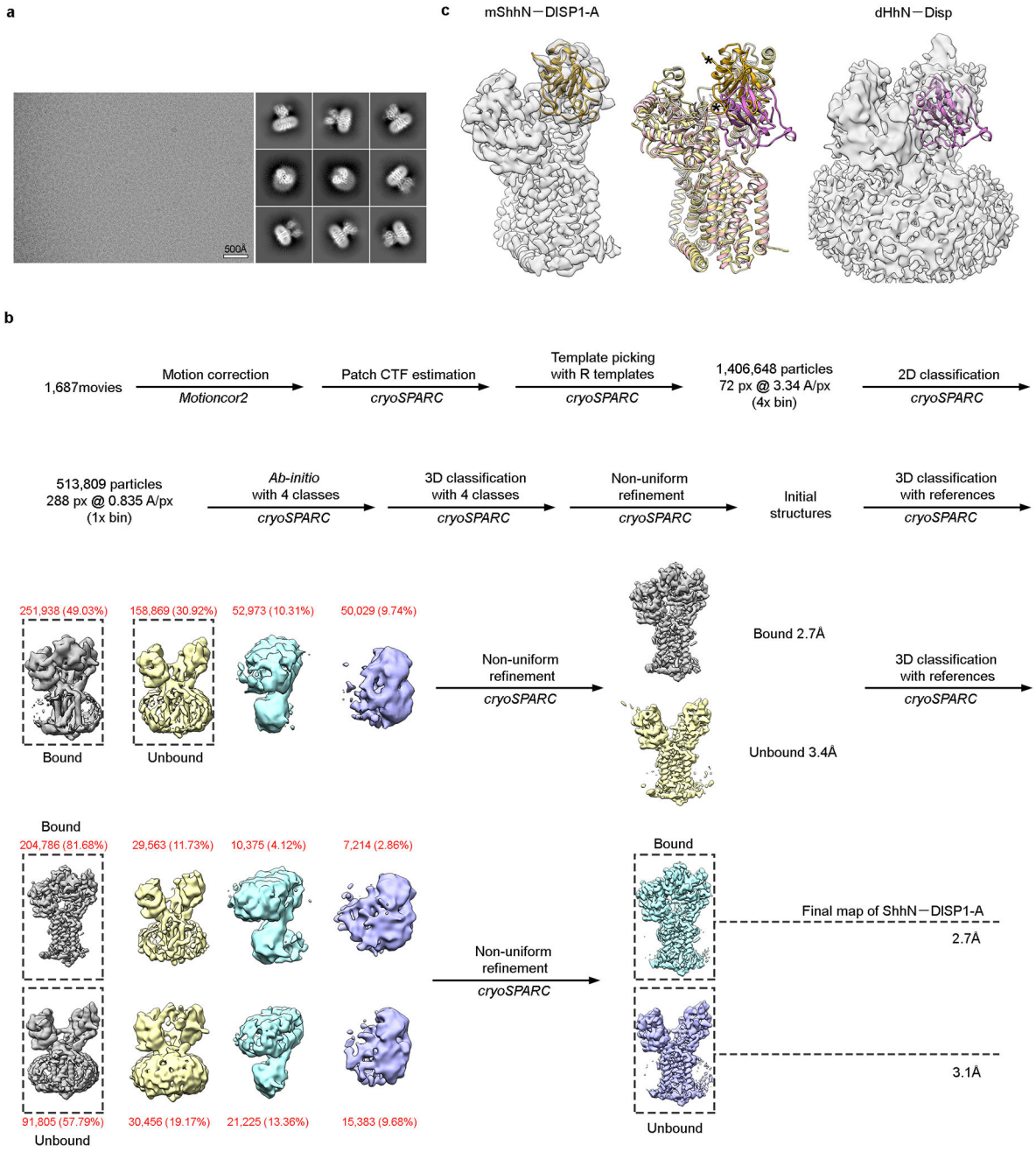

Extended Data Fig. 9 |. Cryo-EM data and image processing flow for ShhN–DISP1-A complex, and comparison to Drosophila HhNDisp complex.

a, A representative cryo-EM micrograph (n = 1687) and highly populated reference-free 2D class averages for ShhN–DISP1-A. **b**, Schematic flow-chart illustrating the image processing used for ShhN–DISP1-A data. Thumbnail images are shown for reference-based 3D classes and high resolution refinements. Dashed black boxes indicate 3D classes selected for the next processing step, with class particle counts in red and refinement GS-FSC resolutions in black. The label, '3D classification with references' indicates that explicit 'apo' and 'complex'references were used to seed the classification. **c**, Left, the

cryo-EM density from our ShhN–DISP1-A complex (transparent grey), overlaid on a ribbon diagram of ShhN (goldenrod). Right, cryo-EM density from the Drosophila HhNDisp complex in Cannac et al[24]. (transparent grey, EMD: 10464), overlaid on the ribbon diagram of HhN (orchid, model extracted from PDB ID: 6TD6). Middle, superimposition of the ShhN–DISP1-A and HhNDisp complex models reported here and in Cannac et al.[24], with mouse DISP1-A and ShhN in khaki and goldenrod, and Drosophila Disp and HhN in pink and orchid. The model of Drosophila HhN was based on docking of a Drosophila HhN structure[56] within a 4.8 Å density map. Relative to Drosophila HhN, murine ShhN is translated upwards, away from the membrane, and rotated towards the right. Asterisks indicate corresponding positions near the N termini of ShhN and HhN proteins. This difference is somewhat puzzling in light of the ability of mammalian DISP1 to rescue Drosophila disp mutant function[6], and we cannot definitively account for it. One functional difference is that mammalian DISP1 cooperates with SCUBE2 for its Hedgehog-releasing activity, whereas Drosophila lacks a Scube orthologue. The ECD domain split and the Hedgehog interaction with the furin-cleaved linker arm together help explain the requirement for furin cleavage[22] in DISP1 function.

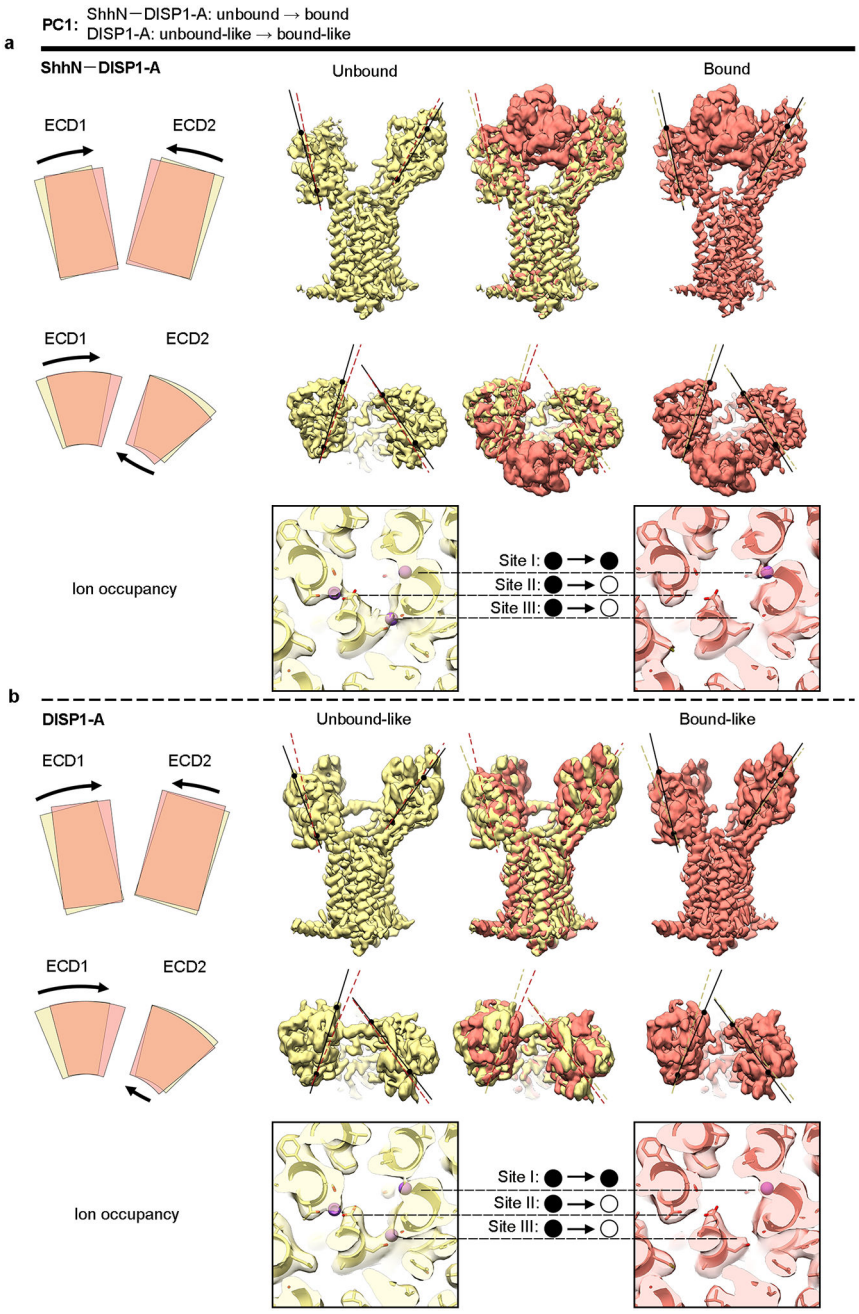

Extended Data Fig. 10 |. Conformational dynamics link intramembrane Na^+ site occupancy to Hedgehog release.

a, Three-dimensional variability analysis (3DVA) of the ShhN–DISP1-A complex dataset reveals a conformational series with ShhN bound or absent at opposite ends of the first principal component (PC1). Front (first line) and top (second line) views of reconstructed densities from the extremes of PC1 (unbound, khaki; bound, salmon) are shown, with a superimposed view of these extremes in the centre. The overall changes in ECD position are illustrated by lines drawn atop the reconstructed densities and by schematized diagrams to the left. Reconstructed densities at the Na^+ coordination sites in the transmembrane domain indicate that these sites change from fully occupied in the unbound state to site I only

occupied in the bound state. See also Supplementary Video 4. b, 3DVA analysis of the apoprotein preparation shows a similar conformational series along PC1, along with similar shifts in Na^+ site occupancy.

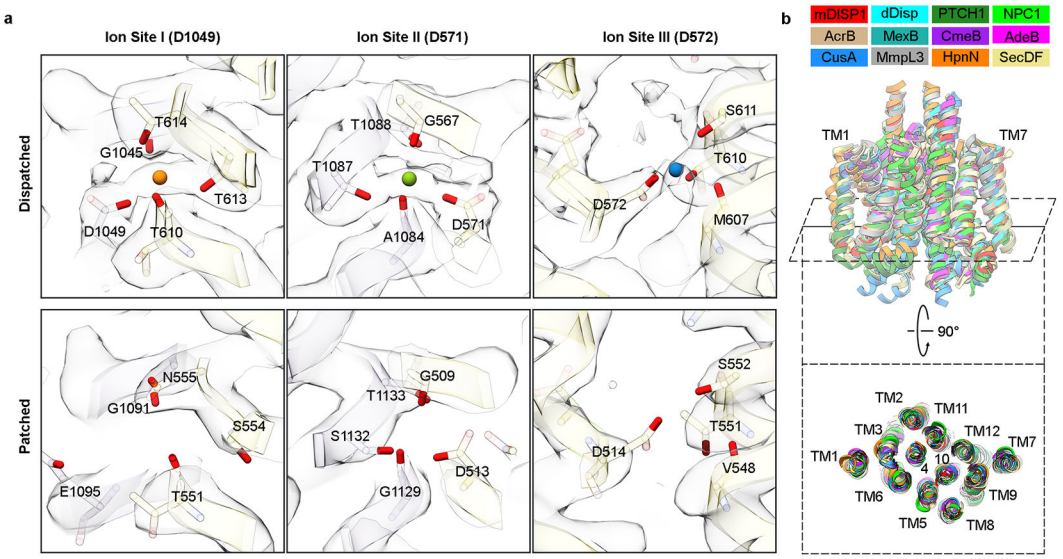

c

Ion Site I (D1049) Ion Site II (D571) Ion Site III (D572) Carbonyl Side chains Charge-neutralizing residues

	TM4	TM5	TM10	TM11	Charge neut (*)	Side-chain ligands(●)	Na^+/H^+	Structural or sequence alignment	Comments
DISP1/Mmus	GIGADD	MFVTSFTT	GLSVD	AALTT	3	10	Na^+	Structure	Export of lipid-modified Hh
Disp/Dmel	GIGADD	MFVTSLTT	GLAVD	AATTT	3	10	Na^+?	Structure[24]	Export of lipid-modified Hh
DISP2/Mmus	GVCVNY	LLVSGLTT	GLSVD	TTGVL	1	6	?	Sequence	Non-functional in Hh export[6]
PTCH1/Hsap	GVGVDD	VALTSISN	GIGVE	GAVST	3	10	Na^+[27]	Structure (6RMG)[35]	Cholesterol transporter[1], regulates Smo in 1° cilium
PTCH2/Mmus	GIGVDD	VALTSVNN	GIGVE	GAVST	3	10	Na^+?	Sequence	Regulates Smo[32]
NPC1/Hsap	AVGVDN	MFLSSFSE	GISVE	GITLT	2	8	?	Structure (6UOX)[57]	Cholesterol transporter[2], Na^+[58] or H^+
NPC1L1/Mmus	AVGVDN	MLLCSLSE	GMSVE	GVAMT	2	8	?	Sequence	Cellular cholesterol absorption[59], Na^+ or H^+
PTCHD1/Mmus	GHGLYG	FSLTTAMY	NYTID	SYLCY	1	7	?	Sequence	Autism gene[60]
PTCHD2/Mmus	GIGVDD	TFFTSLTT	GSSVD	SALTT	3	10	?	Sequence	DISP-like
PTCHD3/Mmus	GVGVDD	ITITTITN	GFSFD	SAIST	3	10	?	Sequence	In sperm tail[61], modified cilium
PTCHD4/Mmus	GHGTKG	YTMTSSLY	NFAID	NITSF	1	6	?	Sequence	Regulated by p53 [62]
AcrB/Ecol	GLLVDD	LVGIAMVL	GLSAK	TSLAF	2	4	H^+	Structure (2GIF)[63]	Trimer, transports antibiotics[63]
MexB/Paer	GLLVDD	LVGIAMVL	GLSAK	TSLAF	2	4	H^+	Structure (2V50)[64]	Trimer, may transport detergents[64]
CmeB/Cjej	GIVVDD	VISIVLVL	GLSAK	TSLAF	2	4	H^+	Structure (5LQ3)[65]	Trimer, transports antibiotics[65]
AdeB/Abau	GIIVDD	IIGITLVL	GLSAK	TSLAF	2	5	H^+	Structure (6OWS)[66]	Trimer, transports antibiotics[66]
CusA/Ecol	GAMVDA	LFISLLII	GVAAE	TVAVI	2	3	H^+	Structure (3NE5)[67]	Trimer, transports Cu^+/Ag^+[67]
MmpL3/Msme	GIAIDY	VVFSAVII	GLSTD	TGAAL	2	4	H^+	Structure (6OR2)[68]	Monomer, transports lipids[68]
HpnN/Bmul	GLGVDF	LALATTAV	GVGVA	SAATT	1	4	H^+	Structure (5KHN)[69]	Dimer, transports hopanoids[69]
SecDF/Tthe2	GAAVDG	IMDVNIAH	GYSIN	TSLTT	1	6	H^+[70]	Structure (3AQP)[70]	Monomer, protein translocation[70]
SecDF1/Valg	GMAVDA	IADANITT	GYSLN	TSGTT	1	7	Na^+[71]	Sequence	Encoded in two proteins (SecD1 and SecF1)[71]

Extended Data Fig. 11 |. Na^+ ion utilization by DISP1, PTCH1, and other members of the RND transporter family.

a, Close-up views of Na^+ ion sites I, II, and III in DISP1, showing the locations of liganding oxygens from amino acid side chains and main-chain carbonyls (see main text), and of the corresponding locations in PTCH1[35] (PDB ID: 6RMG), based on structural alignment of the two proteins. Note the presence in both proteins of a charge-

neutralizing acidic residue at each site, and the conservation of side-chain oxygens as ligands. **b**, Structural alignment, using Chimera Matchmaker, of RND family members, including DISP1, PTCH1, NPC1, and several prokaryotic RND transporters. **c**, Tabulated conservation of charge-neutralizing residues (3 total) or oxygen ligands from amino acid side-chains (10 total) in the indicated proteins, aligned from structure (**b**, see PDB IDs from the second right column) or, if possible without ambiguity, aligned from sequence. References to specific sequences, structures, or background information are given within the table, including refs .[1,2,6,24,27,32,35,57–71]. Note the close conservation of Na^+-liganding side-chains and charge-neutralizing residues in PTCH1, known to require Na^+ for its activity, and in Disp from Drosophila melanogaster. The prokaryotic Na^+-utilizing SecD1/SecF1 peptide translocator from *Vibrio alginolyticus* (encoded as two peptides; aligned by homology to Thermus thermophilus SecDF), in contrast, appears to have evolved a distinct mode of Na^+ interaction. See Supplementary Discussion. Abbreviations: Mmus, *Mus musculus*; Dmel, *Drosophila melanogaster*; Hsap, *Homo sapiens*; Ecol, *Escherichia coli*; Paer, *Pseudomonas aeruginosa*; Cjej, *Campylobacter jejuni*; Abau, *Acinetobacter baumannii*; Msme, *Mycolicibacterium smegmatis*; Bmul, *Burkholderia multivorans*; Tthe2, *Thermus thermophilus*; Valg, *Vibrio alginolyticus*.

Extended Data Table 1.

Cryo-EM data collection, refinement and validation statistics.

	DISP1-A 'R'	DISP1-A 'T'	DISP1-A-NNN	DISP1-A–ShhN Complex
Data collection and processing				
Magnification	EFTEM 105,000	EFTEM 105,000	EFTEM 105,000	EFTEM 105,000
Voltage (kV)	300	300	300	300
Electron exposure (e−/Å^2)	66.7	66.7	65.5	66.7
Defocus range (μm)	−0.5–1.5	−0.5–1.5	−0.5–1.5	−0.5–1.5
Pixel size (Å)	0.835	0.835	0.834	0.835
Symmetry imposed	C1	C1	C1	C1
Initial particle images (no.)	3,717,941	3,717,941	3,489,403	1,406,648
Final particle images (no.)	166,203	154,908	55,982	204,786
Map resolution (Å)	2.49	2.54	3.20	2.71
FSC threshold	0.143	0.143	0.143	0.143
Map resolution range (Å)				
Refinement				
Initial model used (PDB code)	Ab initio	Ab initio	Ab initio	Ab initio
Model resolution (Å)	2.64	2.73	4.25	2.83
FSC threshold	0.5	0.5	0.5	0.5
Model resolution range (Å)				
Map sharpening B factor (Å^2)	−69.9	−72.1	−116.7	−105.6
Model composition				
Non-hydrogen atoms	8,573	8,526	7,926	9,994
Protein residues	926	926	926	1104
Ligands	28	28	14	28

	DISP1-A 'R'	DISP1-A 'T'	DISP1-A-NNN	DISP1-A–ShhN Complex
B factors (Å^2)				
Protein	54/133/76	30/140/87	30/265/180	30/147/77
Ligand	61/114/88	72/140/95	74/250/101	30/120/93
R.m.s. deviations				
Bond lengths (Å)	0.056	0.063	0.048	0.058
Bond angles (°)	2.409	2.316	2.049	2.200
Validation				
MolProbity score	1.02	0.81	1.44	0.87
Clashscore	2.22	1.05	3.26	0.60
Poor rotamers (%)	0.61	0.12	0.98	0.21
Ramachandran plot				
Favored (%)	97.93	98.04	95.42	96.99
Allowed (%)	2.07	1.96	4.47	3.01
Disallowed (%)	0	0	0.11	0

Supplementary Material

Refer to Web version on PubMed Central for supplementary material.

Acknowledgements

We thank K. Roberts and A. Kershner for technical assistance and advice, and V. Korkhov and X. Li for sharing data and information prior to publication. Y.C. is an investigator of the Howard Hughes Medical Institute. Supported by NIH grants R01GM102498, Stanford Department of Urology, and Ludwig Cancer Institute (to P.A.B.) and R35GM140847, S10OD020054 and S10OD021741 (to Y.C.).

Data availability

Coordinates for the DISP1-A R conformation, DISP1-A T conformation, DISP1-A-NNN, and ShhN–DISP1-A complex models reported in this paper have been deposited in the Protein Data Bank under accessions 7RPH, 7RPI, 7RPJ and 7RPK, respectively. The maps of DISP1-A R conformation, DISP1-A T conformation, DISP1-A-NNN and ShhN–DISP1-A complex have been deposited in the Electron Microscopy Data Bank under accession codes EMD-24614, EMD-24615, EMD-24616 and EMD-24617, respectively. Further information and requests for data should be directed to the corresponding authors. PDB IDs of cited structures are provided either in the related figure legends or in the Methods.

References

1. Zhang Y et al. Structural basis for cholesterol transport-like activity of the Hedgehog receptor Patched. Cell 175, 1352–1364.e14 (2018). [PubMed: 30415841]
2. Carstea ED et al. Niemann-Pick C1 disease gene: homology to mediators of cholesterol homeostasis. Science 277, 228–31 (1997). [PubMed: 9211849]
3. Nikaido H & Takatsuka Y Mechanisms of RND multidrug efflux pumps. Biochim. Biophys. Acta 1794, 769–781 (2009). [PubMed: 19026770]

4. Yamaguchi A, Nakashima R & Sakurai K Structural basis of RND-type multidrug exporters. Front. Microbiol 6, 327 (2015). [PubMed: 25941524]
5. Burke R et al. Dispatched, a novel sterol-sensing domain protein dedicated to the release of cholesterol-modified Hedgehog from signaling cells. Cell 99, 803–815 (1999). [PubMed: 10619433]
6. Ma Y et al. Hedgehog-mediated patterning of the mammalian embryo requires transporter-like function of Dispatched. Cell 111, 63–75 (2002). [PubMed: 12372301]
7. Kawakami T et al. Mouse dispatched mutants fail to distribute hedgehog proteins and are defective in hedgehog signaling. Development 129, 5753–5765 (2002). [PubMed: 12421714]
8. Roessler E et al. Truncating loss-of-function mutations of DISP1 contribute to holoprosencephaly-like microform features in humans. Hum. Genet 125, 393–400 (2009). [PubMed: 19184110]
9. Caspary T et al. Mouse dispatched homolog1 is required for long-range, but not juxtacrine, Hh signaling. Curr. Biol 12, 1628–1632 (2002). [PubMed: 12372258]
10. Nakano Y et al. Inactivation of dispatched 1 by the chameleon mutation disrupts Hedgehog signalling in the zebrafish embryo. Dev. Biol 269, 381–392 (2004). [PubMed: 15110707]
11. Riddle RD, Johnson RL, Laufer E & Tabin C Sonic hedgehog mediates the polarizing activity of the ZPA. Cell 75, 1401–1416 (1993). [PubMed: 8269518]
12. Echelard Y et al. Sonic hedgehog, a member of a family of putative signaling molecules, is implicated in the regulation of CNS polarity. Cell 75, 1417–1430 (1993). [PubMed: 7916661]
13. Krauss S, Concordet J-P & Ingham PW A functionally conserved homolog of the Drosophila segment polarity gene hh is expressed in tissues with polarizing activity in Zebrafish embryos. Cell 75, 1431–1444 (1993). [PubMed: 8269519]
14. Chiang C et al. Cyclopia and defective axial patterning in mice lacking Sonic hedgehog gene function. Nature 383, 407–413 (1996). [PubMed: 8837770]
15. Mann RK & Beachy PA Novel lipid modifications of secreted protein signals. Annu. Rev. Biochem 73, 891–923 (2004). [PubMed: 15189162]
16. Porter JA, Young KE & Beachy PA Cholesterol modification of Hedgehog signaling proteins in animal development. Science 274, 255–260 (1996). [PubMed: 8824192]
17. Pepinsky RB et al. Identification of a palmitic acid-modified form of human sonic Hedgehog. J. Biol. Chem 273, 14037–14045 (1998). [PubMed: 9593755]
18. Chamoun Z et al. Skinny Hedgehog, an acyltransferase required for palmitoylation and activity of the Hedgehog signal. Science 293, 2080–2085 (2001). [PubMed: 11486055]
19. Woods IG & Talbot WS The you gene encodes an EGF-CUB protein essential for Hedgehog signaling in Zebrafish. Plos Biol 3, e66 (2005). [PubMed: 15660164]
20. Creanga A et al. Hedgehog signal in soluble form Scube/You activity mediates release of dually lipid-modified Hedgehog signal in soluble form. Genes Dev 26, 1312–1325 (2012). [PubMed: 22677548]
21. Tukachinsky H, Kuzmickas RP, Jao CY, Liu J & Salic A Dispatched and Scube mediate the efficient secretion of the cholesterol-modified Hedgehog ligand. Cell Rep 2, 308–20 (2012). [PubMed: 22902404]
22. Stewart DP et al. Cleavage activates Dispatched for Sonic Hedgehog ligand release. Elife 7, e31678 (2018). [PubMed: 29359685]
23. Punjani A & Fleet DJ 3D variability analysis: resolving continuous flexibility and discrete heterogeneity from single particle cryo-EM. J. Struct. Biol 213, 107702 (2021). [PubMed: 33582281]
24. Cannac F et al. Cryo-EM structure of the Hedgehog release protein Dispatched. Sci. Adv 6, eaay7928 (2020).
25. Chen H, Liu Y & Li X Structure of human Dispatched-1 provides insights into Hedgehog ligand biogenesis. Life Sci. Alliance 3, e202000776 (2020). [PubMed: 32646883]
26. Zheng H et al. CheckMyMetal : a macromolecular metal-binding validation tool. Acta Crystallogr D Struct Biol 73, 223–233 (2017). [PubMed: 28291757]

27. Myers BR, Neahring L, Zhang Y & Roberts KJ Rapid, direct activity assays for Smoothened reveal Hedgehog pathway regulation by membrane cholesterol and extracellular sodium. Proc. Natl Acad. Sci.S 114, E11141–E11150 (2017).
28. Petrov K, Wierbowski BM, Liu J & Salic A Distinct cation gradients power cholesterol transport at different key points in the Hedgehog signaling pathway. Dev. Cell 55, 314–327.e7 (2020). [PubMed: 32860743]
29. Chovancova E et al. CAVER 3.0: a tool for the analysis of transport pathways in dynamic protein structures. PLoS Comput. Biol 8, e1002708 (2012). [PubMed: 23093919]
30. Hall TMT, Porter JA, Beachy PA & Leahy DJ A potential catalytic site revealed by the 1.7–Å crystal structure of the amino–terminal signalling domain of Sonic hedgehog. Nature 378, 212–216 (1995). [PubMed: 7477329]
31. McLellan JS et al. The mode of Hedgehog binding to Ihog homologues is not conserved across different phyla. Nature 455, 979–983 (2008). [PubMed: 18794898]
32. Zhulyn O, Nieuwenhuis E, Liu CY, Angers S & Hui C Ptch2 shares overlapping functions with Ptch1 in Smo regulation and limb development. Dev. Biol 397, 191–202 (2015). [PubMed: 25448692]
33. Deshpande I et al. Smoothened stimulation by membrane sterols drives Hedgehog pathway activity. Nature 571, 284–288 (2019). [PubMed: 31263273]
34. Qi X et al. Cryo-EM structure of oxysterol-bound human Smoothened coupled to a heterotrimeric Gi. Nature 571, 279–283 (2019). [PubMed: 31168089]
35. Qi C, Di Minin G, Vercellino I, Wutz A & Korkhov VM Structural basis of sterol recognition by human hedgehog receptor PTCH1. Sci. Adv 5, eaaw6490 (2019).
36. Whalen DM, Malinauskas T, Gilbert RJC & Siebold C Structural insights into proteoglycan-shaped Hedgehog signaling. Proc. Natl Acad. Sci. USA 110, 16420–16425 (2013). [PubMed: 24062467]
37. Mastronarde DN Automated electron microscope tomography using robust prediction of specimen movements. J. Struct. Biol 152, 36–51 (2005). [PubMed: 16182563]
38. Zheng SQ et al. MotionCor2 : anisotropic correction of beam-induced motion for improved cryo-electron microscopy. Nat. Methods 14, 331–332 (2017). [PubMed: 28250466]
39. Punjani A, Rubinstein JL, Fleet DJ & Brubaker MA cryoSPARC : algorithms for rapid unsupervised cryo-EM structure determination. Nat. Methods 14, 290–296 (2017). [PubMed: 28165473]
40. Zivanov J et al. New tools for automated high-resolution cryo-EM structure determination in RELION-3. Elife 7, e42166 (2018). [PubMed: 30412051]
41. Asarnow D, Palovcak E & Cheng Y 10.5281/zenodo.3576630. (2019).
42. Dang S et al. Cryo-EM structures of the TMEM16A calcium-activated chloride channel. Nature 552, 426–429 (2017). [PubMed: 29236684]
43. Emsley P, Lohkamp B, Scott WG & Cowtan K Features and development of Coot. Acta Crystallogr. D Biol. Crystallogr D66, 486–501 (2010).
44. Adams PD et al. PHENIX : a comprehensive Python-based system for macromolecular structure solution. Acta Crystallogr. D Biol. Crystallogr D66, 213–221 (2010).
45. Croll TI ISOLDE : a physically realistic environment for model building into low-resolution electron-density maps. Acta Crystallogr D Struct Biol D74, 519–530 (2018).
46. Kelley LA, Mezulis S, Yates CM, Wass MN & Sternberg MJE The Phyre2 web portal for protein modelling, prediction and analysis. Nat. Protoc 10, 845–858 (2015). [PubMed: 25950237]
47. Berman H, Henrick K & Nakamura H Announcing the worldwide Protein Data Bank. Nat. Struct. Biol 10, 980 (2003). [PubMed: 14634627]
48. Pettersen EF et al. UCSF Chimera — A visualization system for exploratory research and analysis. J. Comput. Chem 25, 1605–1612 (2004). [PubMed: 15264254]
49. Goddard TD et al. UCSF ChimeraX : meeting modern challenges in visualization and analysis. Protein Sci 27, 14–25 (2018). [PubMed: 28710774]
50. Krissinel E & Henrick K Inference of macromolecular assemblies from crystalline state. J. Mol. Biol 372, 774–797 (2007). [PubMed: 17681537]

51. Sievers F et al. Fast, scalable generation of high-quality protein multiple sequence alignments using Clustal Omega. Mol. Syst. Biol 7, (2011).
52. Robert X & Gouet P Deciphering key features in protein structures with the new ENDscript server. Nucleic Acids Res 42, W320–W324 (2014). [PubMed: 24753421]
53. Goodrich LV, Milenkovic L, Higgins KM & Scott MP Altered neural cell fates and medulloblastoma in mouse patched mutants. Science 277, 1109–1113 (1997). [PubMed: 9262482]
54. Zhang XM, Ramalho-santos M & McMahon AP Smoothened mutants reveal redundant roles for Shh and Ihh signaling including regulation of L/R asymmetry by the mouse node. Cell 105, 781–792 (2001). [PubMed: 11440720]
55. Zhang Y et al. Hedgehog pathway activation through nanobody-mediated conformational blockade of the Patched sterol conduit. Proc. Natl. Acad. Sci. USA 117, 28838–28846 (2020). [PubMed: 33139559]
56. McLellan JS et al. Structure of a heparin-dependent complex of Hedgehog and Ihog. Proc. Natl Acad. Sci. USA 103, 17208–13 (2006). [PubMed: 17077139]
57. Qi X, Hassan A, Liang Q, De Brabander JK & Li X. Structural basis for itraconazole-mediated NPC1 inhibition. Nat. Commun 11, 152 (2020). [PubMed: 31919352]
58. Wang X et al. TPC proteins are phosphoinositide-activated sodium-selective ion channels in endosomes and lysosomes. Cell 151, 372–383 (2012). [PubMed: 23063126]
59. Altmann SW et al. Niemann-Pick C1 like 1 protein is critical for intestinal cholesterol absorption. Science 303, 1201–1204 (2004). [PubMed: 14976318]
60. Chaudhry A et al. Phenotypic spectrum associated with PTCHD1 deletions and truncating mutations includes intellectual disability and autism spectrum disorder. Clin Genet 88, 224–233 (2015). [PubMed: 25131214]
61. Fan J et al. Male germ cell-specific expression of a novel Patched-domain containing gene Ptchd3. Biochem. Biophys. Res. Commun 363, 757–761 (2007). [PubMed: 17904097]
62. Chung JH, Larsen AR, Chen E & Bunz F A PTCH1 homolog transcriptionally activated by p53 suppresses Hedgehog signaling. J. Biol. Chem 289, 33020–33031 (2014). [PubMed: 25296753]
63. Seeger MA et al. Structural asymmetry of AcrB trimer suggests a peristaltic pump mechanism. Science 313, 1295–1298 (2006). [PubMed: 16946072]
64. Sennhauser G, Bukowska MA, Briand C & Grütter MG Crystal Structure of the Multidrug Exporter MexB from Pseudomonas aeruginosa. J. Mol. Biol 389, 134–145 (2009). [PubMed: 19361527]
65. Su C et al. Structures and transport dynamics of a Campylobacter jejuni multidrug efflux pump. Nat. Commun 8, 171 (2017). [PubMed: 28761097]
66. Su C et al. Cryo-electron microscopy structure of an Acinetobacter baumannii multidrug efflux pump. MBio 10, e01295–19 (2019). [PubMed: 31266873]
67. Su C et al. Crystal structure of the CusBA heavy-metal efflux complex of Escherichia coli. Nature 470, 558–562 (2011). [PubMed: 21350490]
68. Su C et al. MmpL3 is a lipid transporter that binds trehalose monomycolate and phosphatidylethanolamine. Proc. Natl Acad. Sci. USA 116, 11241–11246 (2019). [PubMed: 31113875]
69. Kumar N, Su C, Chou T, Radhakrishnan A & Delmar JA Crystal structures of the Burkholderia multivorans hopanoid transporter HpnN. Proc. Natl Acad. Sci. USA 114, 6557–6562 (2017). [PubMed: 28584102]
70. Tsukazaki T et al. Structure and function of a membrane component SecDF that enhances protein export. Nature 474, 235–8 (2011). [PubMed: 21562494]
71. Ishii E et al. Nascent chain-monitored remodeling of the Sec machinery for salinity adaptation of marine bacteria. Proc. Natl Acad. Sci. USA 112, E5513–22 (2015). [PubMed: 26392525]

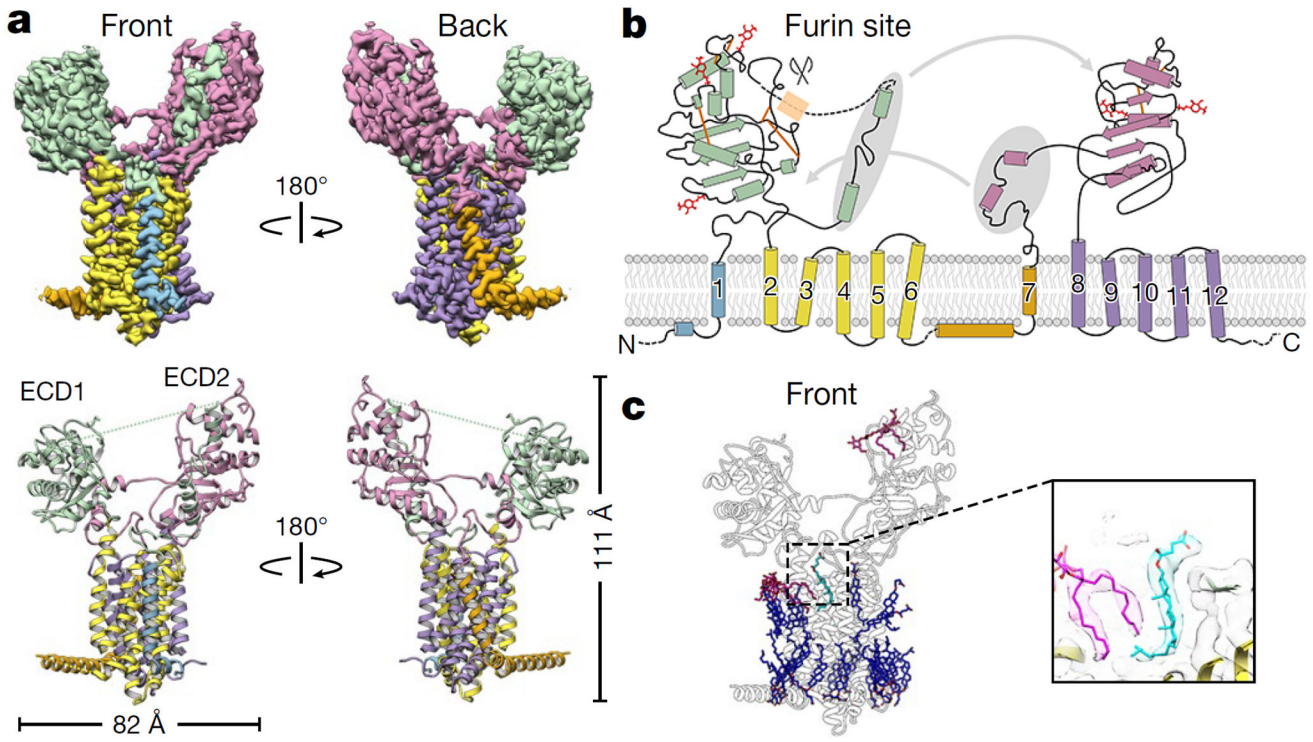

Fig. 1 |. Structure and lipid binding sites of DISP1.

a, b, Corresponding views of the cryo-EM map (top) and atomic model (bottom) of DISP1-A (the R conformation, as seen by 3D classification and 3DVA) (Extended Data Figs. 3–5). Domains are coloured as follows: pre-TM1 helix and TM1, blue; TM1–TM2 loop, lime; TM2–TM6, yellow; pre-TM7 and TM7, orange; TM7–TM8 loop, pink; TM8–TM12, lavender. **b**, Topology diagram of DISP1-A showing secondary structure elements (same colours as in **a**), disulfide bonds (gold lines), glycosylation sites (red symbols) and unresolved regions (black dashed lines, amino acid residues 1, 2, 172, 173, 264–282, 399–409, 667–680 and 1144–1521); (Extended Data Fig. 2). Secondary elements exchanged between extracellular loops to form ECD1 and ECD2 are highlighted by oval shadows. **c**, Front view of DISP1-A (pale ribbon) with resolved LMNG (magenta) and CHS (blue) molecules (see also Supplementary Video 2). A sterol molecule (cyan) located at the front of DISP1 is positioned above other sterols in the outer leaflet and is shown in the magnified inset (right) as a stick model with corresponding density and an associated, tilted LMNG molecule (magenta); this lifted sterol may correspond to an intermediate in the extraction of Hedgehog-associated lipids from the membrane.

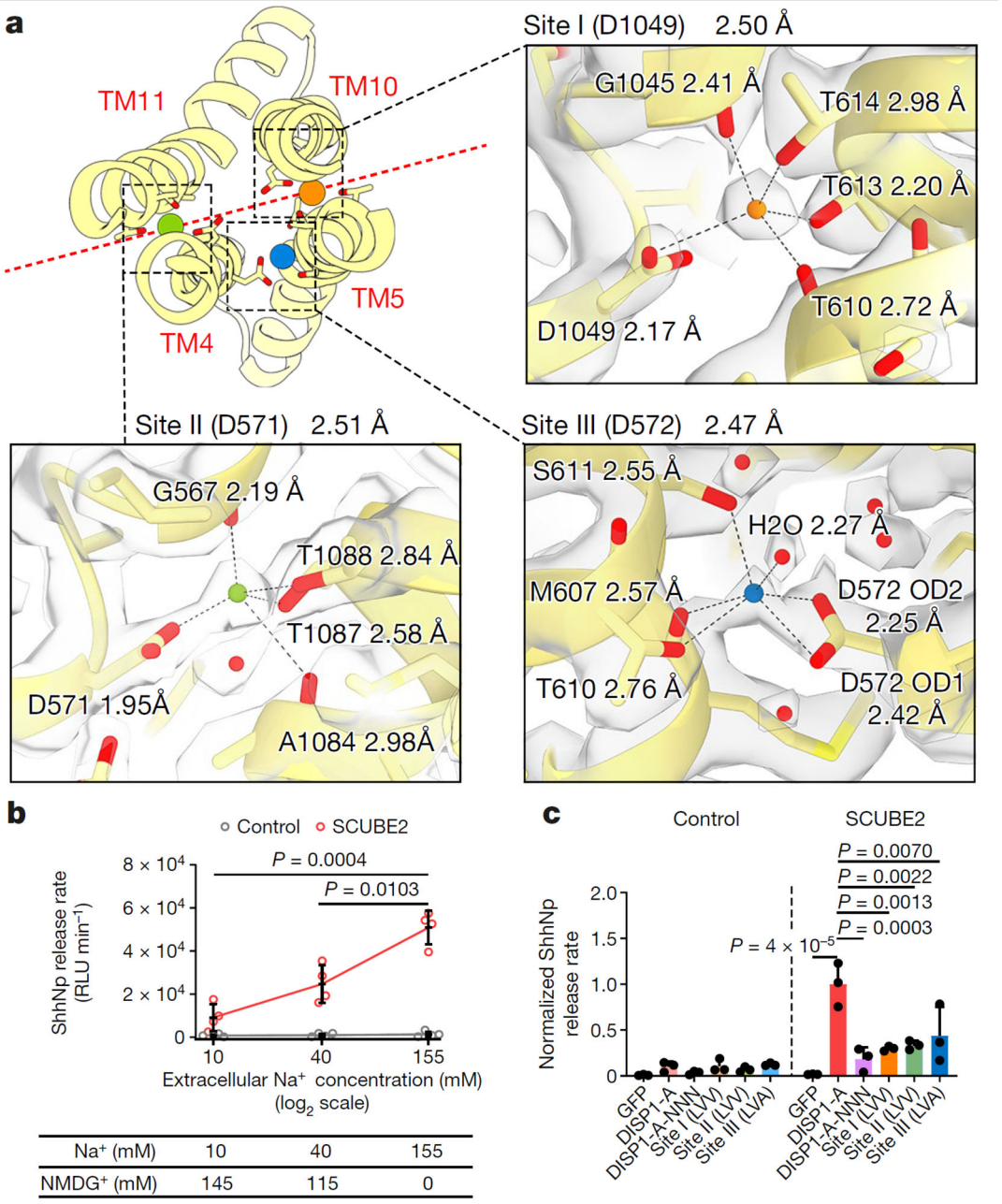

Fig. 2 |. Three Na^+ densities in the transmembrane domain.

a, Close-up views of the full set of coordinating ligands for each of the three Na+ ions are shown with protein-derived densities superimposed on the atomic model of DISP1-A (overview, top left; dashed red line showing the pseudodyad axis between TM1–TM6 and TM7–TM12). Dashed lines in magnified ion sites denote coordination bonds and corresponding centre-to-centre distances between Na^+ ions and associated oxygens. Contour levels are 6σ for sites I and II, and 5σ for site III. b, c, Na^+-dependent ShhNp release by DISP1. **b**, NanoLuc-ShhNp released from $Disp^{-/-}$ mouse embryonic fibroblasts (MEFs) transfected to express DISP1-A–mEGFP and NanoLuc–ShhNp, and incubated in defined

medium at different Na^+ concentrations, with or without (control) purified SCUBE2 protein (mouse SCUBE2 lacking amino acids 30–281). $NMDG^+$ was added to maintain osmolarity for Na^+ concentrations below 155 mM (Extended Data Fig. 8c). Slopes from linear regression applied to the linear portions of normalized NanoLuc–ShhNp release data were used to calculate release rates (Methods, Extended Data Fig. 8d). NanoLuc–ShhNp release was critically dependent on the Na^+ gradient. NanoLuc–ShhNp release was normalized to DISP1, ShhNp and total protein. RLU, relative luminescence units. **c**, Impaired NanoLuc–ShhNp release (measured as in **b**) for DISP1-A (normalized to 1.0) and variants with alterations disrupting Na^+ binding at all three sites (DISP1-A-NNN, D571N/D572N/D1049N) or individually, at site I (LVV, D1049L/T613V/T614V), site II (LVV, D571L/T1087V/T1088V) or site III (LVA, D572L/T610V/S611A). SCUBE2 concentrations were 1 μM in **b** (30 min time course), and 0.15 μM in **c** (75 min time course). Data in b and c are mean ± s.d., n = 3 (**c**) or 4 (**b**) biologically independent experiments; statistical analysis for SCUBE2+ conditions (datasets normally distributed) used one-way analysis of variance (ANOVA) with Tukey's test (**b**) or Dunnett's test (**c**, with DISP1-A as comparison).

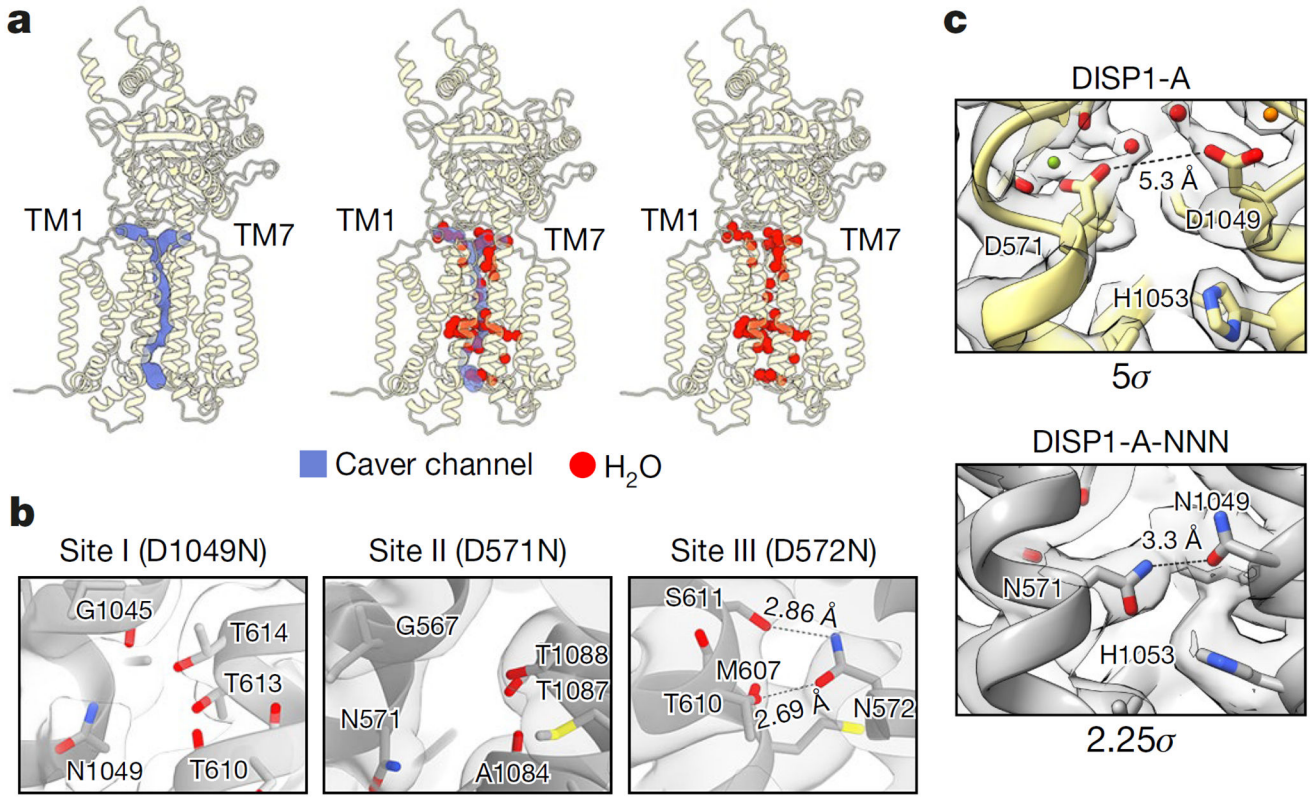

Fig. 3 |. A transmembrane Na^+ permeation channel is disrupted in the structure of DISP1-A-NNN.

a, A continuous pathway through the transmembrane domain of DISP1-A, shown as a purple surface (left), is identified by the Caver 3[29] PyMOL plugin with a probe of radius 1.0 Å, appropriate for the passage of Na^+. This channel is partly occupied by resolved water molecules, shown as red spheres (right; superimposition with Caver channel in centre), and provides access to the transmembrane cavity that contains the Na^+ ions and water (Supplementary Video 3). **b**, Close-up views of the three Na^+ ion sites in the DISP1-A-NNN structure (3.2 Å resolution) show no discernible Na^+ densities, even when contoured at 3σ (Na^+ densities in DISP1-A were clearly seen at ≥5σ for all three sites). Site III in particular has collapsed entirely, with TM4 and TM5 moving close enough to permit D572N to form hydrogen bonds with the side-chains of T610 and S611. **c**, In DISP1-A, D571 and D1049 side chains coordinate and neutralize their respective Na^+ ions, maintaining a minimum distance of 5.3 Å, whereas in DISP1-A-NNN, the absence of Na^+ permits D571N and D1049N side chains to rotate toward and interact across the pseudodyad axis at a reduced distance of 3.3 Å. The motion of D571N together with an upward tilting of H1053 disrupt the connection between the channel and the intracellular exit (Supplementary Discussion).

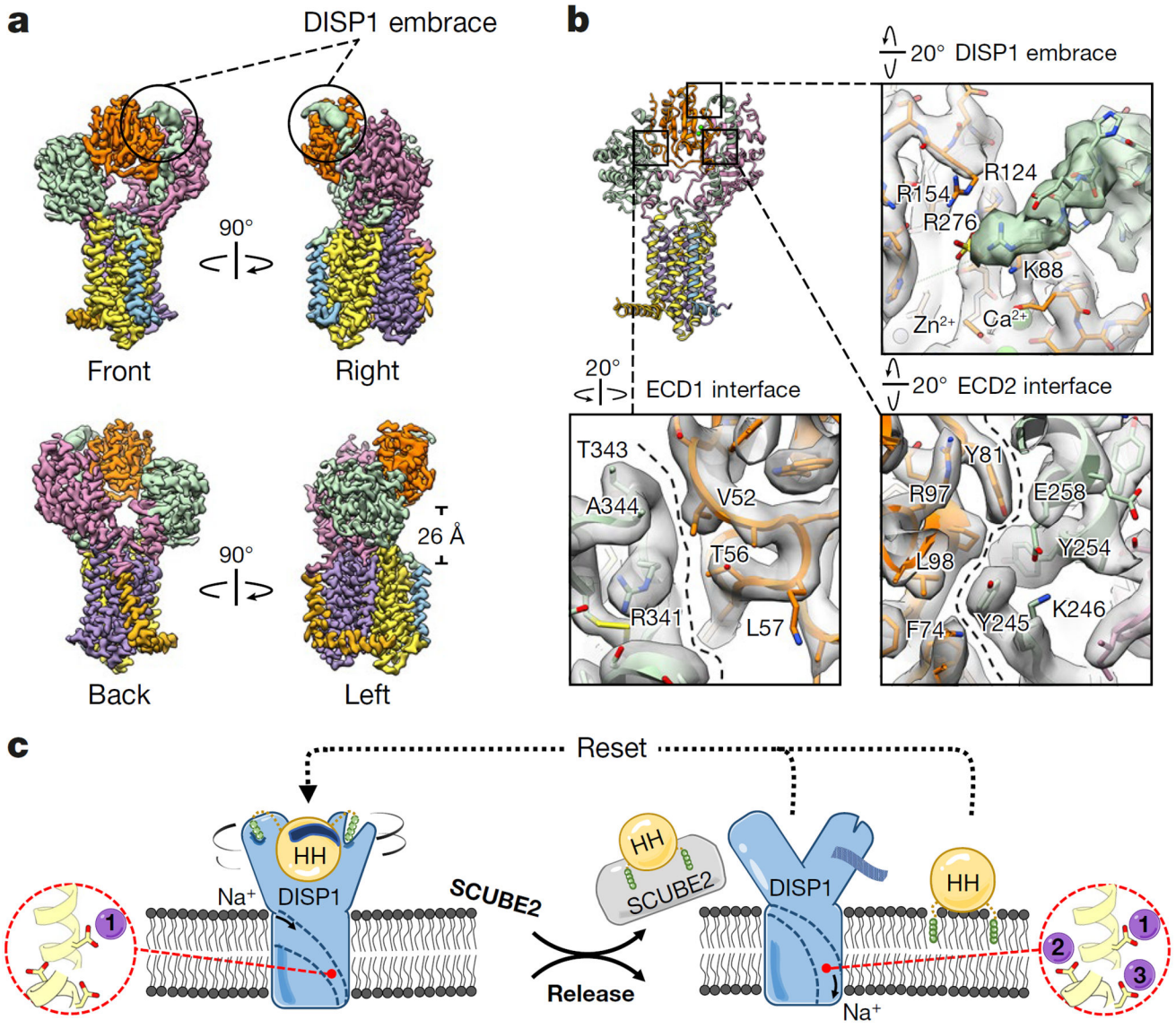

Fig. 4 |. DISP1-A binds ShhN between its distal ECDs.

a, Cryo-EM density map of a ShhN–DISP1-A complex at 2.7 Å resolution enabled de novo modelling of ShhN at a location 26 Å above the transmembrane domain of DISP1-A. ShhN is in orange; DISP1-A colours are as in Fig. 1a. The furin-cleaved linker, although not resolved in the DISP1-A apo structure, is stabilized within the complex and seen to extend from ECD2 in a one-armed molecular embrace of ShhN. The region of ShhN contacted by this linker corresponds to a polybasic region that interacts with heparin sulfate or other sulfated glycosaminoglycans (GAGs)[36], which would be displaced by the DISP1 molecular embrace. **b**, Three major interaction interfaces between ShhN and DISP1-A. The ECD1 and ECD2 interfaces feature primarily van der Waals interactions, with the extensive ECD2 interface additionally including a hydrogen bond between ShhN K75 and the backbone carbonyl of DISP1-A R241 (located just below the expanded view (not shown)). Near the tip of the furin-cleaved linker arm, R276 of DISP1-A forms an ionic interaction with a sulfate ion that also interacts with basic residues in ShhN (R124, R154 and K88). **c**,

A model for Na^+-driven conformational dynamics in the DISP1 activity cycle. Membrane-anchored, dual-lipid-modified Hedgehog protein (HH) is activated for release to SCUBE2 by interaction with DISP1 ECDs. Hedgehog activation (left) entails (1) a pincer-like action of the DISP1 ECDs; (2) interaction with and stabilization of the DISP1 furin-cleaved linker (dark blue); and (3) accommodation of Hedgehog-linked lipids in hydrophobic distal cavities of DISP1 ECDs. From this activated state, associated with restricted Na^+ occupancy (site I only, from 3DVA, ShhN-bound state), SCUBE2 availability and the chemiosmotic force of the transmembrane Na+ gradient together drive Hedgehog release to SCUBE2 and resetting of DISP1 for resumption of the cycle (right) (see Supplementary Video 4).